

RD-A164 155

NUMERICAL FLOW FIELD CALCULATIONS FOR A MISSILE  
CONFIGURATION AT  $M = 6$ (U) ARMY BALLISTIC RESEARCH LAB  
ABERDEEN PROVING GROUND MD J SAHU ET AL JAN 86

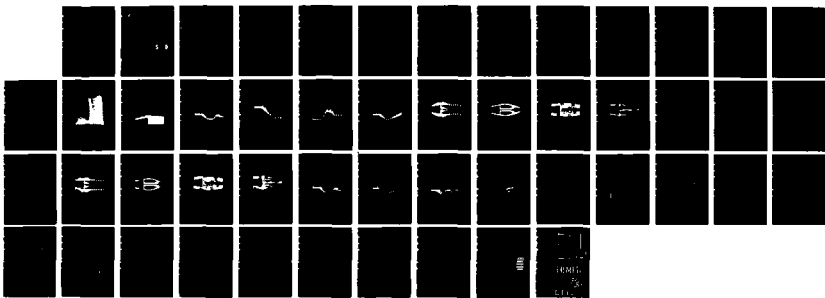
1/1

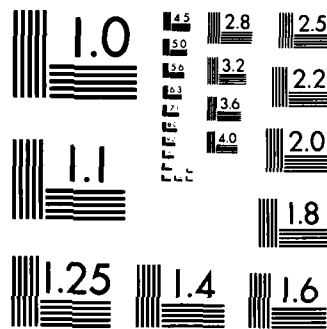
UNCLASSIFIED

BRL-MR-3491

F/G 28/4

NL





MICROCOPY RESOLUTION TEST CHART  
STANDARDS-1963-A

AD-A164 155

12



US ARMY  
MATERIEL  
COMMAND

AD

MEMORANDUM REPORT BRL-MR-3491

NUMERICAL FLOW FIELD CALCULATIONS FOR  
A MISSILE CONFIGURATION AT  $M = .6$

Jubaraj Sahu  
Charles J. Nietubicz

January 1986

DTIC  
ELECTED  
FEB 13 1986  
S D  
X D

APPROVED FOR PUBLIC RELEASE; DISTRIBUTION UNLIMITED.

US ARMY BALLISTIC RESEARCH LABORATORY  
ABERDEEN PROVING GROUND, MARYLAND

DTIC FILE COPY

0 2 13 035

Destroy this report when it is no longer needed.  
Do not return it to the originator.

Additional copies of this report may be obtained  
from the National Technical Information Service,  
U. S. Department of Commerce, Springfield, Virginia  
22161.

The findings in this report are not to be construed as an official  
Department of the Army position, unless so designated by other  
authorized documents.

The use of trade names or manufacturers' names in this report  
does not constitute indorsement of any commercial product.

UNCLASSIFIED

---

SECURITY CLASSIFICATION OF THIS PAGE (When Data Entered)

REPORT DOCUMENTATION PAGE		READ INSTRUCTIONS BEFORE COMPLETING FORM
1. REPORT NUMBER <b>Memorandum Report BRL-MR-3491</b>	2. GOVT ACCESSION NO. <b>AD-A164155</b>	3. RECIPIENT'S CATALOG NUMBER
4. TITLE (and Subtitle) <b>NUMERICAL FLOW FIELD CALCULATIONS FOR A MISSILE CONFIGURATION AT M = .6</b>	5. TYPE OF REPORT & PERIOD COVERED <b>FINAL</b>	
7. AUTHOR(s) <b>Jubaraj Sahu and Charles J. Nietubicz</b>	8. CONTRACT OR GRANT NUMBER(s)	
9. PERFORMING ORGANIZATION NAME AND ADDRESS <b>U.S. Army Ballistic Research Laboratory ATTN: SLCBR-LF Aberdeen Proving Ground, MD 21005-5066</b>	10. PROGRAM ELEMENT, PROJECT, TASK AREA & WORK UNIT NUMBERS <b>RDT&amp;E 1L162618AH80</b>	
11. CONTROLLING OFFICE NAME AND ADDRESS <b>U.S. Army Ballistic Research Laboratory ATTN: SLCBR-DD-T Aberdeen Proving Ground, MD 21005-5066</b>	12. REPORT DATE <b>January 1986</b>	
14. MONITORING AGENCY NAME & ADDRESS (if different from Controlling Office)	13. NUMBER OF PAGES <b>47</b>	
16. DISTRIBUTION STATEMENT (of this Report)	15. SECURITY CLASS. (of this report) <b>UNCLASSIFIED</b>	
	15a. DECLASSIFICATION/DOWNGRADING SCHEDULE	
17. DISTRIBUTION STATEMENT (of the abstract entered in Block 20, if different from Report)		
18. SUPPLEMENTARY NOTES <b>This report supersedes IMR 831 dated December 1984.</b>		
19. KEY WORDS (Continue on reverse side if necessary and identify by block number)		
<b>Navier-Stokes Computations Missile Flow Field Separation Regions Finite-Difference Scheme</b>	<b>Turbulent Flow Subsonic Speed Implicit Algorithm</b>	
20. ABSTRACT (Continue on reverse side if necessary and identify by block number)	<p>Large separated flow region can seriously degrade the effectiveness of fins or any other control surface located in that region. A knowledge of the expected flow field can thus be very important in the initial design phase of a missile or projectile. The Aerodynamics Technology Branch of the US Army Missile Laboratory has requested numerical flow field data for a new missile design. Numerical computations have been made for the requested missile configuration at <math>M = 0.6</math> and the results of these computations are presented in</p>	

UNCLASSIFIED

SECURITY CLASSIFICATION OF THIS PAGE(When Data Entered)

20. ABSTRACT (Continued)

this report.

A thin-layer Navier-Stokes base flow code has been used to compute the flow field for a full missile configuration including the base region. Numerical calculations have been made for both laminar and turbulent flow conditions. Details of the computed flow field are presented in the form of plots showing surface pressure distribution, velocity vectors, stream function and Mach number contours, particle paths and boundary layer parameters.

UNCLASSIFIED

SECURITY CLASSIFICATION OF THIS PAGE(When Data Entered)

## TABLE OF CONTENTS

	<u>Page</u>
LIST OF ILLUSTRATIONS.....	5
I. INTRODUCTION.....	7
II. COMPUTATIONAL TECHNIQUE.....	7
III. RESULTS.....	10
A. Case 1, $Re = 4.2 \times 10^6/\text{ft}$ (Turbulent Flow).....	10
B. Case 2, $Re = 3.0 \times 10^6/\text{ft}$ (Turbulent Flow).....	11
C. Case 3, $Re = 4.2 \times 10^6/\text{ft}$ (Laminar Flow).....	11
IV. CONCLUDING REMARKS.....	12
REFERENCES.....	43
DISTRIBUTION LIST.....	45

Accession For	
NTIS	CRA&I
DTIC	TAB
Unannounced	
Justification _____	
By _____	
Distribution / _____	
Availability Codes	
Dist	Avail and / or Special
A-1	

## LIST OF ILLUSTRATIONS

<u>Figure</u>		<u>Page</u>
1	Expanded View of the Grid Near the Missile.....	13
2	Expanded View of the Grid in the Base Region.....	14
3	Velocity Vectors, $M_{\infty} = 0.6, \alpha = 0$ .....	15
	a. $3.0 < X < 6.0$ .....	15
	b. $3.4 < X < 4.6$ .....	16
	c. $4.6 < X < 6.0$ .....	17
	d. $7.4 < X < 8.6$ .....	18
4	Velocity Vectors in Base Region, $M_{\infty} = 0.6, \alpha = 0,$ $Re = 4.2 \times 10^6/\text{ft}$ (Turbulent).....	19
5	Particle Paths in Base Region, $M_{\infty} = 0.6, \alpha = 0,$ $Re = 4.2 \times 10^6/\text{ft}$ (Turbulent).....	20
6	Mach Number Contours in Base Region, $M_{\infty} = 0.6, \alpha = 0,$ $Re = 4.2 \times 10^6/\text{ft}$ (Turbulent).....	21
7	Static Temperature Contours in Base Region, $M_{\infty} = 0.6, \alpha = 0,$ $Re = 4.2 \times 10^6/\text{ft}$ (Turbulent).....	22
8	Surface Pressure Distribution, $M_{\infty} = 0.6, \alpha = 0,$ $Re = 4.2 \times 10^6/\text{ft}$ (Turbulent).....	23
9	Skin Friction Coefficient Distribution, $M_{\infty} = 0.6, \alpha = 0,$ $Re = 4.2 \times 10^6/\text{ft}$ (Turbulent).....	24
10	Surface Pressure Distribution, $M_{\infty} = 0.6, \alpha = 0,$ $Re = 3.0 \times 10^6/\text{ft}$ (Turbulent).....	25
11	Skin Friction Coefficient Distribution, $M_{\infty} = 0.6, \alpha = 0,$ $Re = 3.0 \times 10^6/\text{ft}$ (Turbulent).....	26
12	Velocity Vectors in Base Region, $M_{\infty} = 0.6, \alpha = 0,$ $Re = 4.2 \times 10^6/\text{ft}$ (Laminar).....	27
13	Particle Paths in Base Region, $M_{\infty} = 0.6, \alpha = 0,$ $Re = 4.2 \times 10^6/\text{ft}$ (Laminar).....	28
14	Mach Number Contours in Base Region, $M_{\infty} = 0.6, \alpha = 0,$ $Re = 4.2 \times 10^6/\text{ft}$ (Laminar).....	29
15	Static Temperature Contours in Base Region, $M_{\infty} = 0.6, \alpha = 0,$ $Re = 4.2 \times 10^6/\text{ft}$ (Laminar).....	30

LIST OF ILLUSTRATIONS (Cont'd)

<u>Figure</u>		<u>Page</u>
16	Velocity Vectors, $M_{\infty} = 0.6$ , $\alpha = 0$ , $Re = 4.2 \times 10^6/\text{ft}$ (Laminar) ..	31
17	Velocity Vectors, $M_{\infty} = 0.6$ , $\alpha = 0$ , $Re = 4.2 \times 10^6/\text{ft}$ (Laminar) ..	32
18	Stream Function Contours, $M_{\infty} = 0.6$ , $\alpha = 0$ , $Re = 4.2 \times 10^6/\text{ft}$ (Laminar) .....	33
19	Stream Function Contours, $M_{\infty} = 0.6$ , $\alpha = 0$ , $Re = 4.2 \times 10^6/\text{ft}$ (Laminar) .....	34
20	Surface Pressure Distribution, $M_{\infty} = 0.6$ , $\alpha = 0$ , $Re = 4.2 \times 10^6/\text{ft}$ (Laminar) .....	35
21	Skin Friction Coefficient Distribution, $M_{\infty} = 0.6$ , $\alpha = 0$ , $Re = 4.2 \times 10^6/\text{ft}$ (Laminar) .....	36
22	Density Profile, $M_{\infty} = .6$ , $\alpha = 0$ , $X/D = 8.306$ .....	37
23	X-Component of Velocity Profile, $M_{\infty} = .6$ , $\alpha = 0$ , $X/D = 8.306$ ....	38
24	Y-Component of Velocity Profile, $M_{\infty} = .6$ , $\alpha = 0$ , $X/D = 8.306$ ....	39
25	Static Pressure Profile, $M_{\infty} = .6$ , $\alpha = 0$ , $X/D = 8.306$ .....	40
26	Dynamic Pressure Profile, $M_{\infty} = .6$ , $\alpha = 0$ , $X/D = 8.306$ .....	41

## I. INTRODUCTION

Surface irregularities such as cavities, bumps and flares, etc., may all be present in actual missile configurations. The resulting flow field for these shapes is characterized by locally separated flow regions due to these surface irregularities. Additionally, large separated flow regions exist behind the base of the missile. These separated flow regions could have a large affect on the missile aerodynamics. Fins and control surfaces are often added to improve the stability. Proper location of these devices are crucial in achieving full effectiveness. The control effectiveness of the fins or other control surfaces can be seriously degraded if they are located in regions of large separated flow. A knowledge of the expected flow field and the boundary layer properties can thus be very important in the initial design phase. The Aerodynamics Technology Branch of the US Army Missile Laboratory has requested numerical flow field data for a new missile design. Numerical computations have been made for the requested missile geometry at  $M = 0.6$ . The results of these computations are presented in this memorandum report.

## II. COMPUTATIONAL TECHNIQUE

The Azimuthal Invariant (or Generalized Axisymmetric) thin-layer Navier-Stokes equations for general spatial coordinates  $\xi$ ,  $\eta$ ,  $\zeta$  can be written as<sup>1</sup>

$$\partial_t \hat{q} + \partial_\xi \hat{E} + \partial_\zeta \hat{G} + \hat{H} = Re^{-1} \partial_\zeta \hat{S} \quad (1)$$

where  $\xi = \xi(x, y, z, t)$  is the longitudinal coordinate

$\eta = \eta(y, z, t)$  is the circumferential coordinate

$\zeta = \zeta(x, y, z, t)$  is the near normal coordinate

$t = t$  is the time

and

$$\hat{q} = J^{-1} \begin{bmatrix} \rho \\ \rho u \\ \rho v \\ \rho w \\ e \end{bmatrix}, \quad \hat{E} = J^{-1} \begin{bmatrix} \rho u \\ \rho u u + \xi_x p \\ \rho v u + \xi_y p \\ \rho w u + \xi_z p \\ (\epsilon + p) u - \xi_t p \end{bmatrix}, \quad \hat{G} = J^{-1} \begin{bmatrix} \rho w \\ \rho w u + \xi_x p \\ \rho v w + \xi_y p \\ \rho w w + \xi_z p \\ (\epsilon + p) w - \xi_t p \end{bmatrix}$$

---

1. C. J. Niestubicz, T. H. Pulliam, and J. L. Steger, "Numerical Solution of the Azimuthal-Invariant Navier-Stokes Equations," U.S. Army Ballistic Research Laboratory, Aberdeen Proving Ground, Maryland, ARBRL-TR-02227, March 1980. (AD A085716) (Also see AIAA Paper No. 79-0010, January 1979.)

$$\hat{H} = J^{-1} \begin{bmatrix} 0 \\ 0 \\ \rho V [R_\xi (U - \xi_t) + R_\zeta (W - \zeta_t)] \\ -\rho V R (V - n_t) - \rho / R \\ 0 \end{bmatrix}$$

$$\hat{S} = \begin{bmatrix} 0 \\ u(\xi_x^2 + \xi_y^2 + \xi_z^2)u_\zeta + (u/3)(\xi_x u_\zeta + \xi_y v_\zeta + \xi_z w_\zeta)\xi_x \\ u(\xi_x^2 + \xi_y^2 + \xi_z^2)v_\zeta + (u/3)(\xi_x u_\zeta + \xi_y v_\zeta + \xi_z w_\zeta)\xi_y \\ u(\xi_x^2 + \xi_y^2 + \xi_z^2)w_\zeta + (u/3)(\xi_x u_\zeta + \xi_y v_\zeta + \xi_z w_\zeta)\xi_z \\ ((\xi_x^2 + \xi_y^2 + \xi_z^2)[(u/2)(u^2 + v^2 + w^2)]_\zeta + \kappa \rho r^{-1}(\gamma - 1)^{-1}(a^2)_z \\ + (u/3)(\xi_x u + \xi_y v + \xi_z w)(\xi_x u_\zeta + \xi_y v_\zeta + \xi_z w_\zeta) \end{bmatrix}$$

The velocities

$$\begin{aligned} U &= \xi_t + \xi_x u + \xi_y v + \xi_z w \\ V &= n_t + n_x u + n_y v + n_z w \\ W &= \zeta_t + \zeta_x u + \zeta_y v + \zeta_z w \end{aligned} \quad (2)$$

represent the contravariant velocity components.

The Cartesian velocity components ( $u$ ,  $v$ ,  $w$ ) are nondimensionalized with respect to  $a_\infty$  (free stream speed of sound). The density ( $\rho$ ) is referenced to  $\rho_\infty$  and total energy ( $e$ ) to  $\rho_\infty a_\infty^2$ . The local pressure is determined using the equation of state,

$$p = (\gamma - 1)[e - 0.5\rho(u^2 + v^2 + w^2)] \quad (3)$$

where  $\gamma$  is the ratio of specific heats.

In Equation (1), axisymmetric flow assumptions have been made which result in the source term,  $\hat{H}$ . The details of how this is obtained can be found in Reference 1 and are not discussed here. Equation (1) contains only two spatial derivatives. However, it retains all three momentum equations and allows a degree of generality over the standard axisymmetric equations. In

particular, the circumferential velocity is not assumed to be zero, thus allowing computations for spinning projectiles to be accomplished.

The numerical algorithm used is the Beam-Warming fully implicit, approximately factored finite difference scheme. The algorithm can be first or second order accurate in time and second or fourth order accurate in space. Since the interest is only in the steady-state solution, Equation (1) is solved in a time asymptotic fashion and first order accurate time differencing is used. The spatial accuracy is fourth order. Details of the algorithm are included in References 2-4.

For the computation of turbulent flows, a turbulence model must be supplied. In the present calculations a two layer algebraic eddy viscosity model by Baldwin and Lomax<sup>5</sup> is used. In their two layer model the inner region follows the Prandtl-Van Driest formulation. Their outer formulation can be used in wakes as well as in attached and separated boundary layers. In both the inner and outer formulations, the distribution of vorticity is used to determine length scales, thereby avoiding the necessity of finding the outer edge of the boundary layer (or wake). The magnitude of the local vorticity for the axisymmetric formulation is given by

$$|\omega| = \sqrt{\left(\frac{\partial u}{\partial x}\right)^2 + \left(\frac{\partial v}{\partial z} - \frac{\partial w}{\partial y}\right)^2 + \left(\frac{\partial w}{\partial x} - \frac{\partial u}{\partial z}\right)^2} . \quad (4)$$

In determining the outer length scale a function<sup>5</sup>

$$F(y) = y|\omega| [1 - \exp(-y^+/A^+)] \quad (5)$$

was used.

The thin-layer Navier-Stokes computational technique described above was used in conjunction with an unique flow field segmentation procedure and a computational capability<sup>6 7</sup> has been recently developed for predicting the

---

2. J. L. Steger, "Implicit Finite Difference Simulation of Flow About Arbitrary Geometries with Application to Airfoils," AIAA Journal, Vol. 16, No. 7, July 1978, pp. 679-686.
3. T. H. Pulliam and J. L. Steger, "On Implicit Finite-Difference Simulations of Three-Dimensional Flow," AIAA Journal, Vol. 18, No. 2, February 1980, pp. 159-167.
4. R. Beam and R. F. Warming, "An Implicit Factored Scheme for the Compressible Navier-Stokes Equations," AIAA Journal, Vol. 16, No. 4, April 1978, pp. 393-402.
5. B. S. Baldwin and H. Lomax, "Thin-Layer Approximation and Algebraic Model for Separated Turbulent Flows," AIAA Paper No. 78-257, 1978.

flow field over a projectile including the base region flow. The flow field segmentation procedure allows the complete numerical simulation of a projectile. The details of this procedure can be found in References 6 and 7. This code is used here to calculate the full flow field over a missile at  $M = 0.6$  and  $\alpha = 0$ .

### III. RESULTS

Numerical computations have been made at two Reynolds Numbers,  $Re = 4.2 \times 10^6/\text{ft}$  and  $3.0 \times 10^6/\text{ft}$  for turbulent flow and  $Re = 4.2 \times 10^6/\text{ft}$  for laminar flow (total length,  $L = 23.63"$ ). Solutions were marched in time until the steady state results were achieved. The lengths shown in results are in calibers (1 caliber = 2.66", the reference diameter).

Figure 1 shows an expanded view of the computational grid near the missile which is approximately 9 calibers long. The grid consists of 201 points in longitudinal direction and 50 points in the normal direction. The dark regions result from grid clustering. These are the regions where the flow variables are expected to change considerably. The expanded grid in the base region is shown in Figure 2 and has been adapted to the wake shear layer as the solution developed. Computed results are now presented for the various cases.

#### A. Case 1, $Re = 4.2 \times 10^6/\text{ft}$ (Turbulent Flow)

Figure 3 shows the velocity vectors in the regions where surface irregularities are present and flow separation may occur. As seen in Figure 3(a) there is a very thin region of reversed flow near the surface. Figure 3(b) and (c) are expanded views of Figure 3(a). Figure 3(d) shows the velocity vectors near the flare and again only a very thin separated flow region is predicted near the missile surface.

Qualitative features of the base region flow field are shown in Figures 4-7. Figure 4 is a plot of the velocity vectors and clearly shows the recirculatory flow in the near wake. Figure 5 shows the particle paths in the base region and more clearly shows the separation bubble. Mach number and normalized static temperature contour plots are shown in Figure 6 and 7, respectively, and show the strong free shear layer. It is clear from Figure 6 that the flow is subsonic everywhere in the base region.

---

6. J. Sahu, C. J. Nietubicz and J. L. Steger, "Numerical Computation of Base Flow for a Projectile at Transonic Speeds," U.S. Army Ballistic Research Laboratory, Aberdeen Proving Ground, Maryland, ARBRL-TR-02495, June 1983. (AD A130293) (Also see AIAA Paper No. 82-1358, August 1982.)
7. J. Sahu, C. J. Nietubicz and J. L. Steger, "Navier-Stokes Computations of Projectile Base Flow with and without Base Injection," U.S. Army Ballistic Research Laboratory, Aberdeen Proving Ground, Maryland, ARBRL-TR-02532, November 1983. (AD A135738) (Also see AIAA Paper No. 83-0224, January 1983.)

Quantitative results are presented in the form of pressure coefficient and skin friction coefficient. Figure 8 shows the surface pressure distribution as a function of the longitudinal position. The flow is subsonic everywhere ( $C_p > C_p^*$ ) and the expansions and recompressions are observed at the cavity, protuberance and flare as expected. The pressure distribution shown downstream of the base corner is along a line following the shear layer. Figure 9 shows the skin friction coefficient distribution and clearly indicates the reversed flow regions where  $C_f < 0$ .

B. Case 2,  $Re = 3.0 \times 10^6/\text{ft}$  (Turbulent Flow)

The results for this case are essentially the same as those of the previous case. Small differences in the surface pressure distribution and skin friction coefficient distribution are observed and these distributions are shown in Figures 10 and 11. The differences are very small and usually occur in the separated flow regions.

C. Case 3,  $Re = 4.2 \times 10^6/\text{ft}$  (Laminar Flow)

Qualitative features of the base region flow field for the laminar flow case are shown in Figures 12-15. Although small differences can be observed, the extent and size of the wake separation bubble remains essentially the same as for the turbulent case. Significant differences in the flow field, however, occur in the regions of the cavity, protuberance and the flare and are shown in Figures 16-19. Figures 16 and 17 show the velocity vectors in these regions and the large separated flow regions are evident. Figures 18 and 19 are stream function contour plots for the same regions and more clearly show the reversed flow. These stream function plots clearly show the separation and reattachment points.

Quantitatively, the surface pressure and the skin friction coefficient distributions are shown in Figures 20 and 21, respectively. As seen in Figure 20, the expansions and the compressions are weak compared to the turbulent case. The magnitude of the skin coefficient shown in Figure 21 is considerably lower than for the turbulent case (Figure 9). Additionally, larger regions of separated flow are clearly seen ( $C_f < 0$ ).

As part of the missile design, fins are located at  $X/D = 8.306$ . The flow field at this location is of considerable importance to the Aerodynamic Technology Branch of the US Army Missile Command. The flow field requested is in terms of plots and tabular data of density, velocity, static pressure and dynamic pressure profiles. Figures 22-26 show the profiles of density, velocity components in streamwise and normal directions, static and dynamic pressures respectively. The tabular data of these profiles are included in Table 1 and includes the following variables:

Z/D	normal distance measured from the surface
RHO/RINF	non-dimensional density
U/UINF	non-dimensional x-component of velocity
W/UINF	non-dimensional y-component of velocity
P/PINF	non-dimensional static pressure
Q/QINF	non-dimensional dynamic pressure

where  $D$  is the reference diameter and  $R_{\text{INF}}$ ,  $U_{\text{INF}}$ ,  $P_{\text{INF}}$  and  $Q_{\text{INF}}$  are the free stream values for density, velocity, static pressure and dynamic pressure respectively.

#### IV. CONCLUDING REMARKS

A thin-layer Navier-Stokes code has been used to compute the entire flow field about a missile configuration of interest to the Aerodynamics Technology Branch of the US Army Missile Laboratory. Numerical computations have been made at  $M_{\infty} = 0.6$  and  $\alpha = 0$  and for both laminar and turbulent flow conditions. Turbulent flow computations indicate very thin regions of separated flow near the missile surface in the neighborhood of the irregularities in surface geometry. The laminar case predicts much larger separated flow regions in the same areas. The flow field in terms of plots and tabular data of density, velocity, static pressure and dynamic pressure at the location of fins are also included.

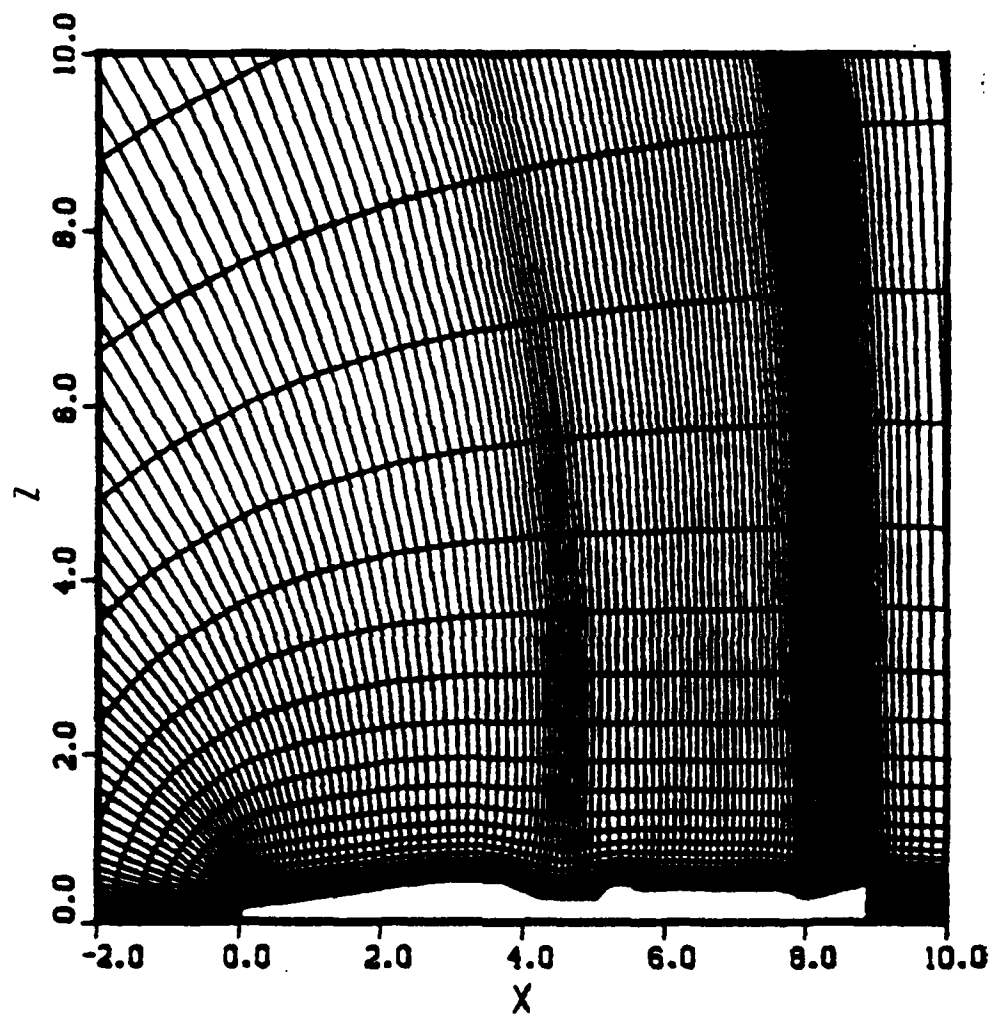


Figure 1. Expanded View of the Grid Near the Missile

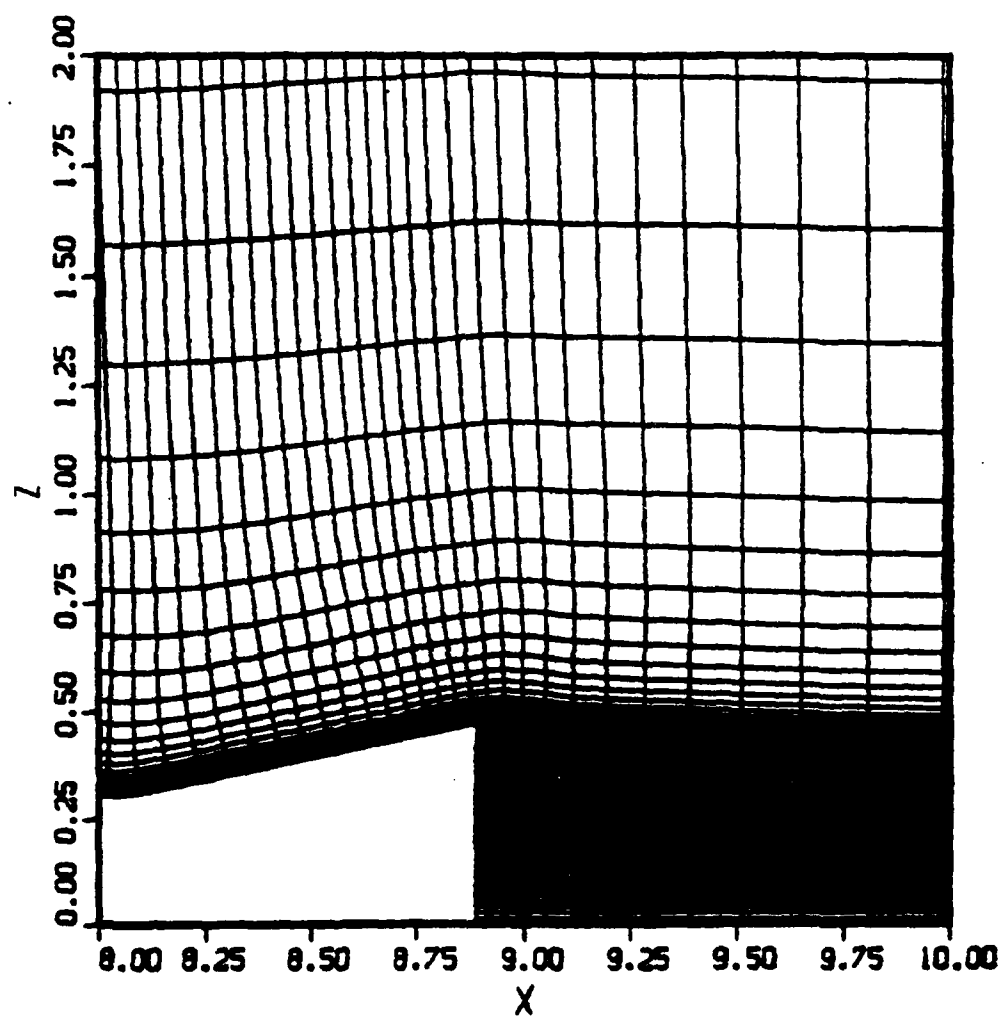


Figure 2. Expanded View of the Grid in the Base Region

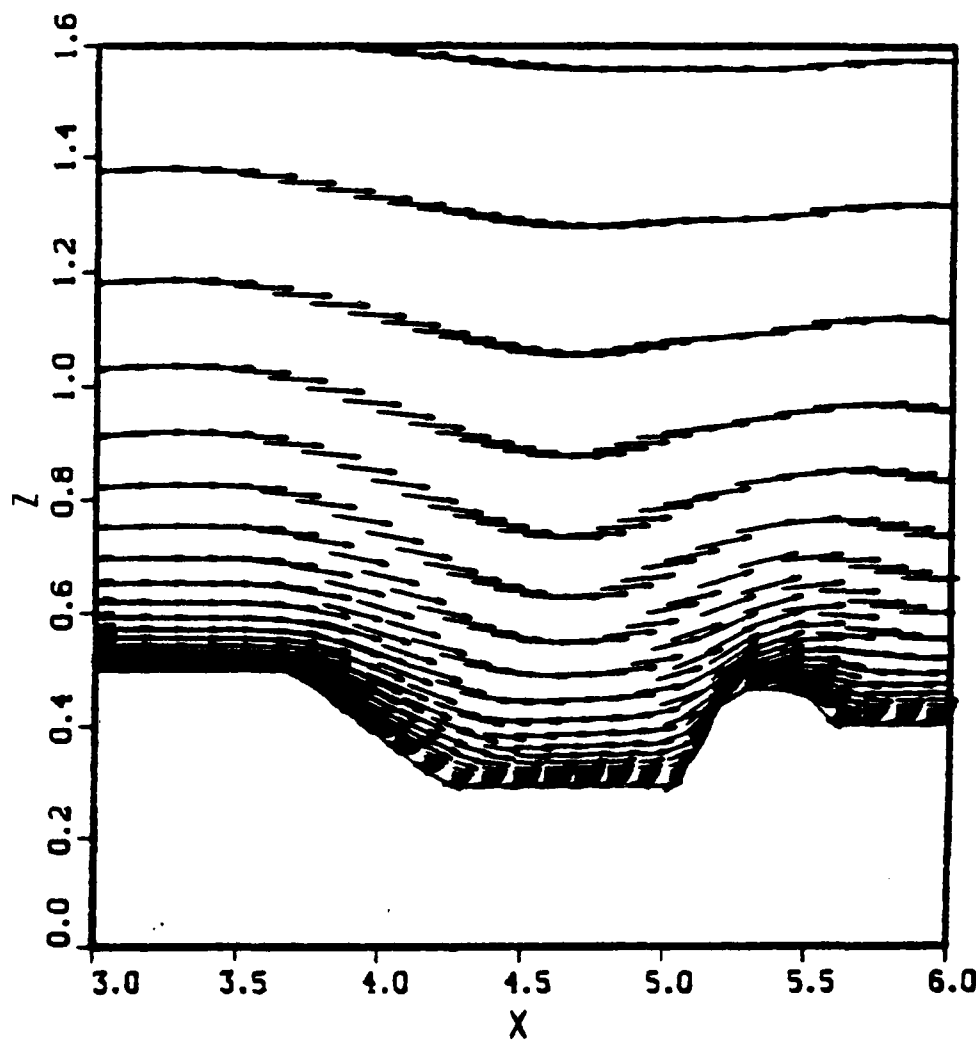


Figure 3. Velocity Vectors,  $M_\infty = 0.6$ ,  $\alpha = 0$

a.  $3.0 < X < 6.0$

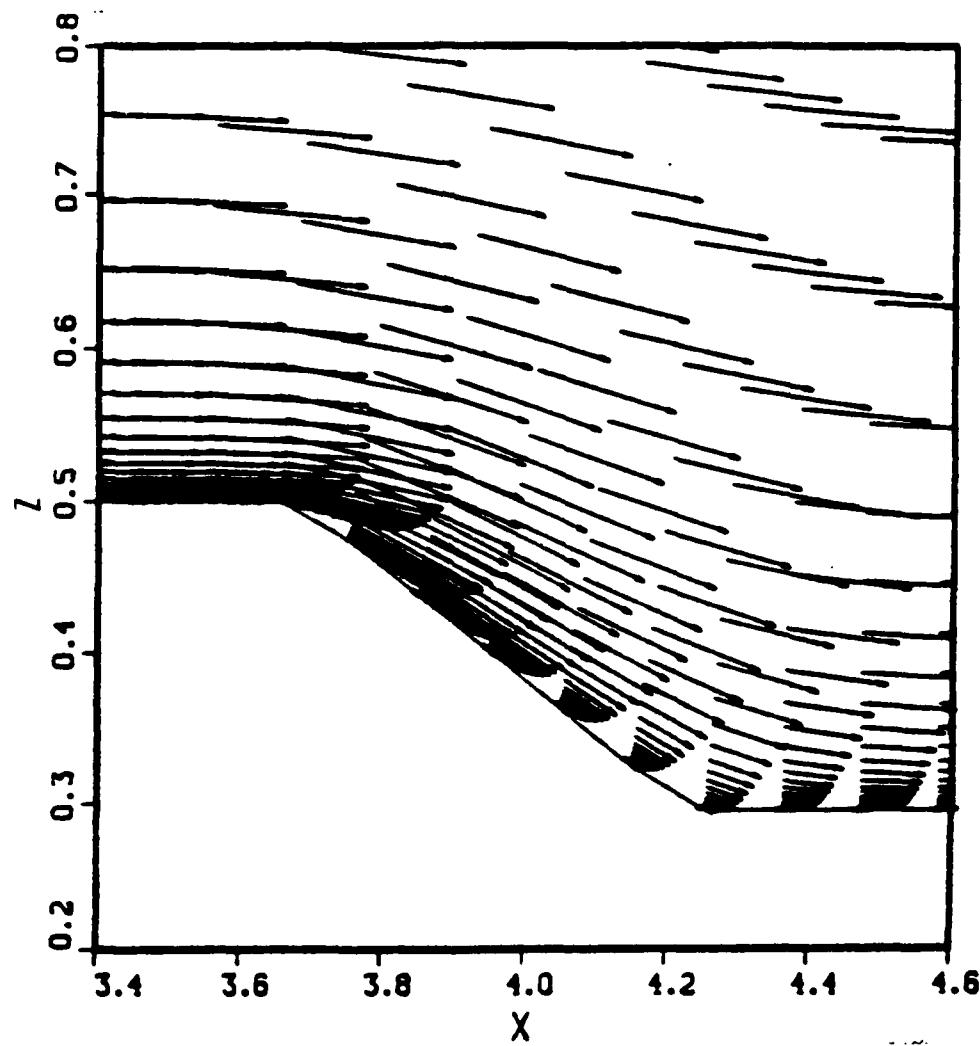


Figure 3. Continued

b.  $3.4 < X < 4.6$

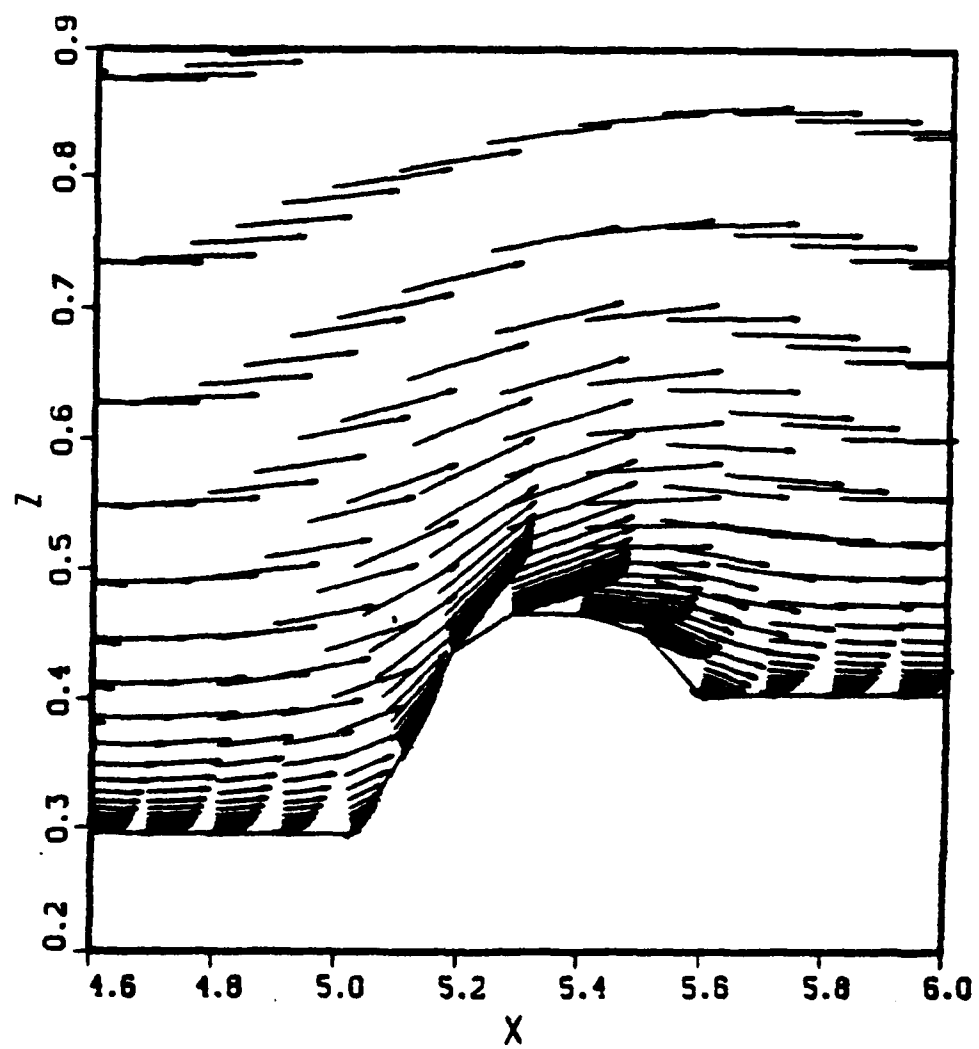


Figure 3. Continued

c.  $4.6 < X < 6.0$

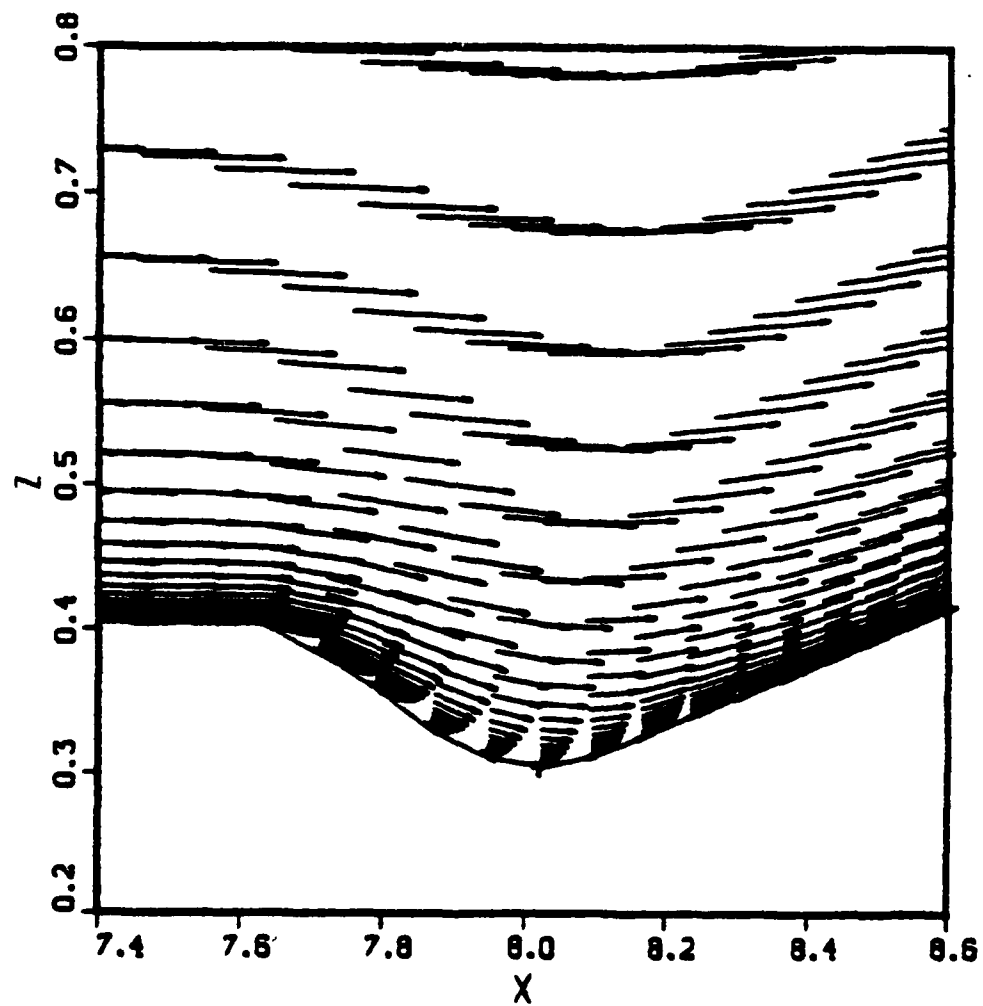


Figure 3. Continued

d.  $7.4 < X < 8.6$

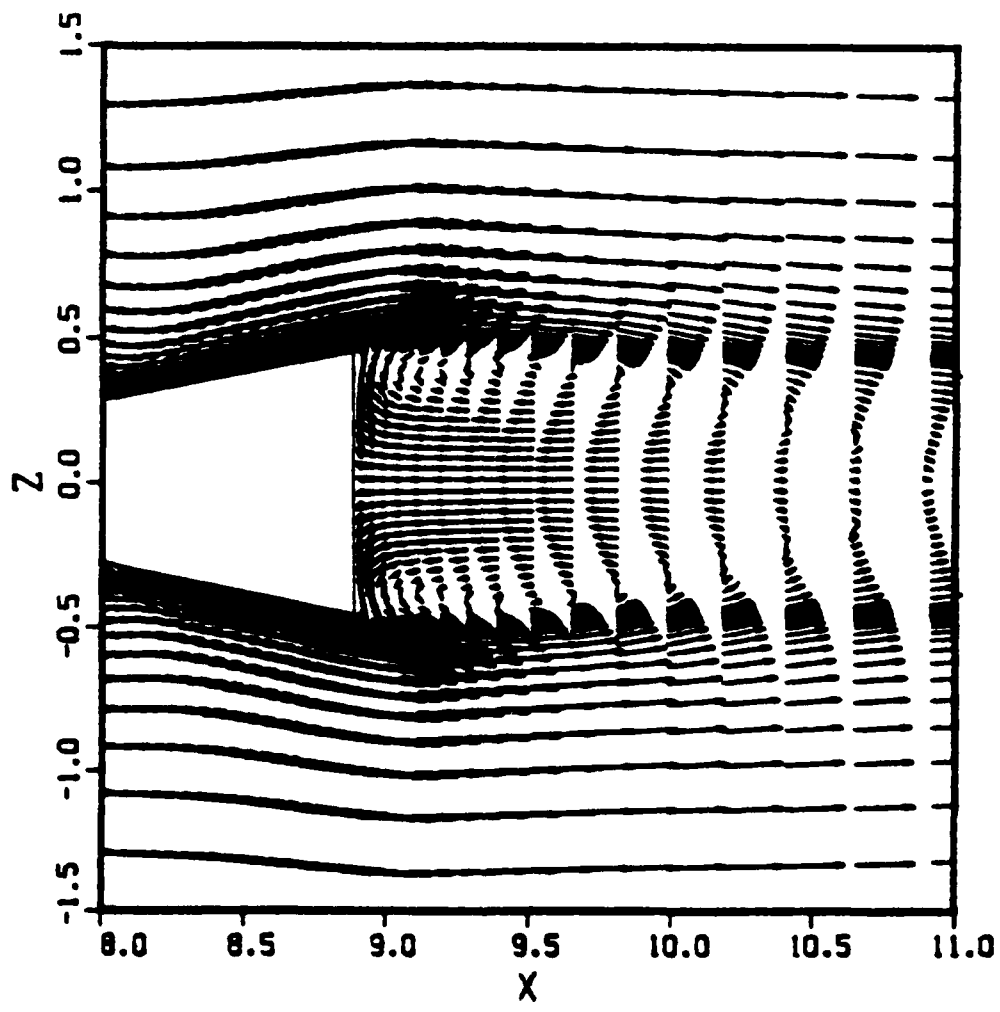


Figure 4. Velocity Vectors in Base Region,  $M_\infty = 0.6$ ,  $\alpha = 0$ ,  
 $Re = 4.2 \times 10^6/\text{ft}$  (Turbulent)

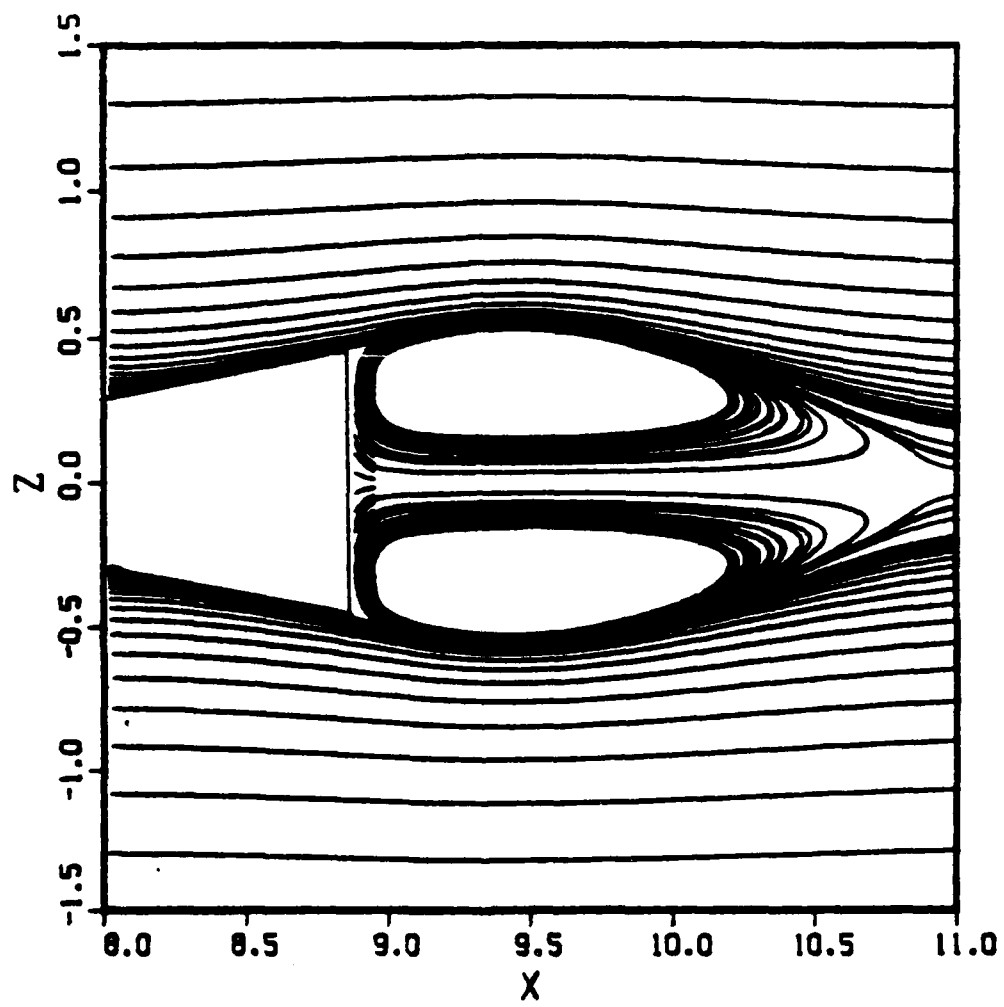


Figure 5. Particle Paths in Base Region,  $M_\infty = 0.6$ ,  $\alpha = 0$ ,  
 $Re = 4.2 \times 10^6/\text{ft}$  (Turbulent)

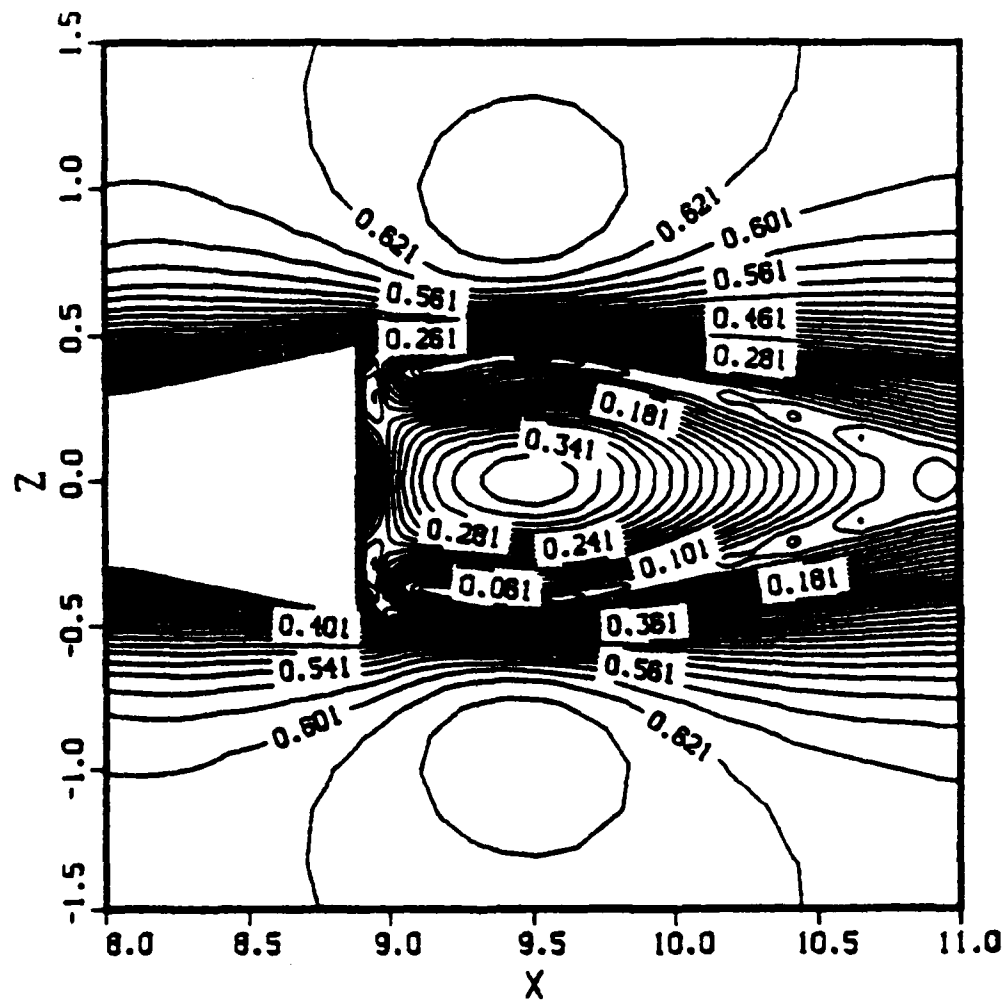


Figure 6. Mach Number Contours in Base Region,  $M_\infty = 0.6$ ,  $\alpha = 0$ ,  
 $Re = 4.2 \times 10^6/\text{ft}$  (Turbulent)

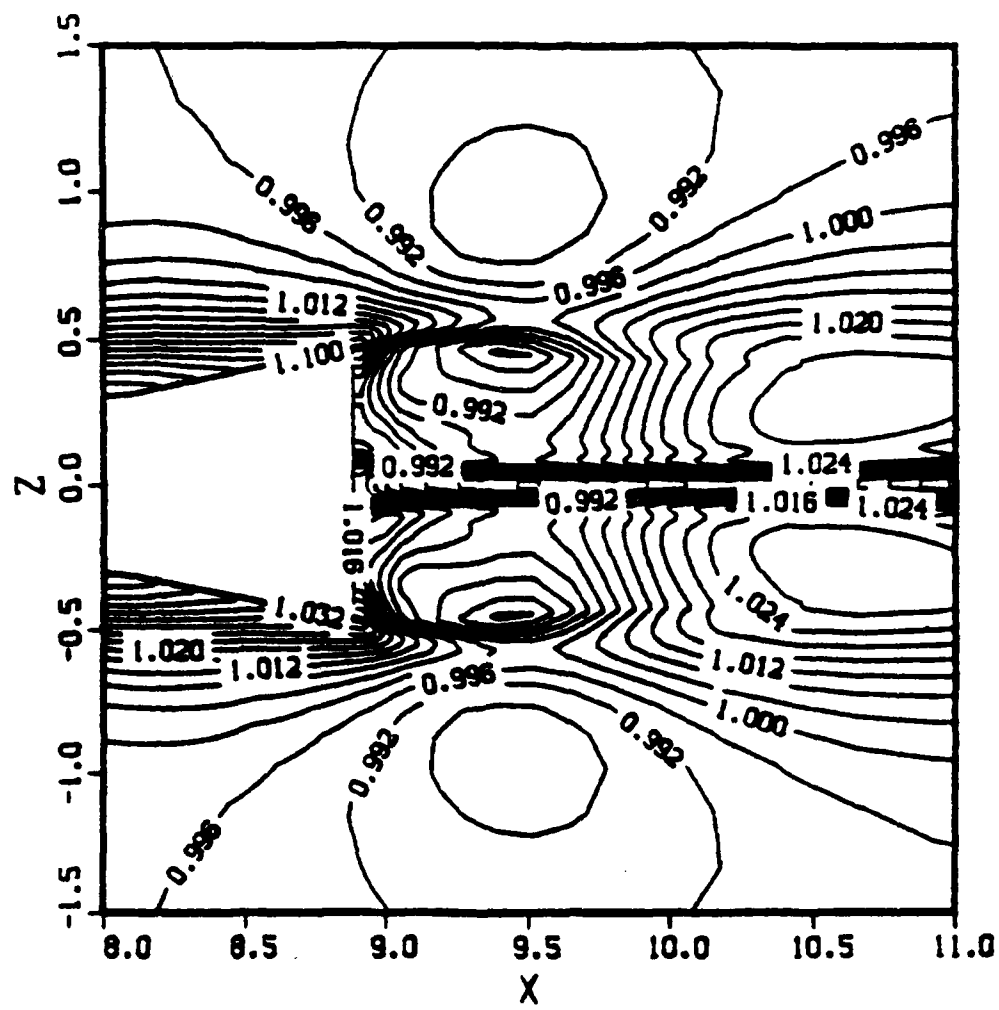


Figure 7. Static Temperature Contours in Base Region,  $M_\infty = 0.6$ ,  $\alpha = 0$ ,  
 $Re = 4.2 \times 10^6/\text{ft}$  (Turbulent)

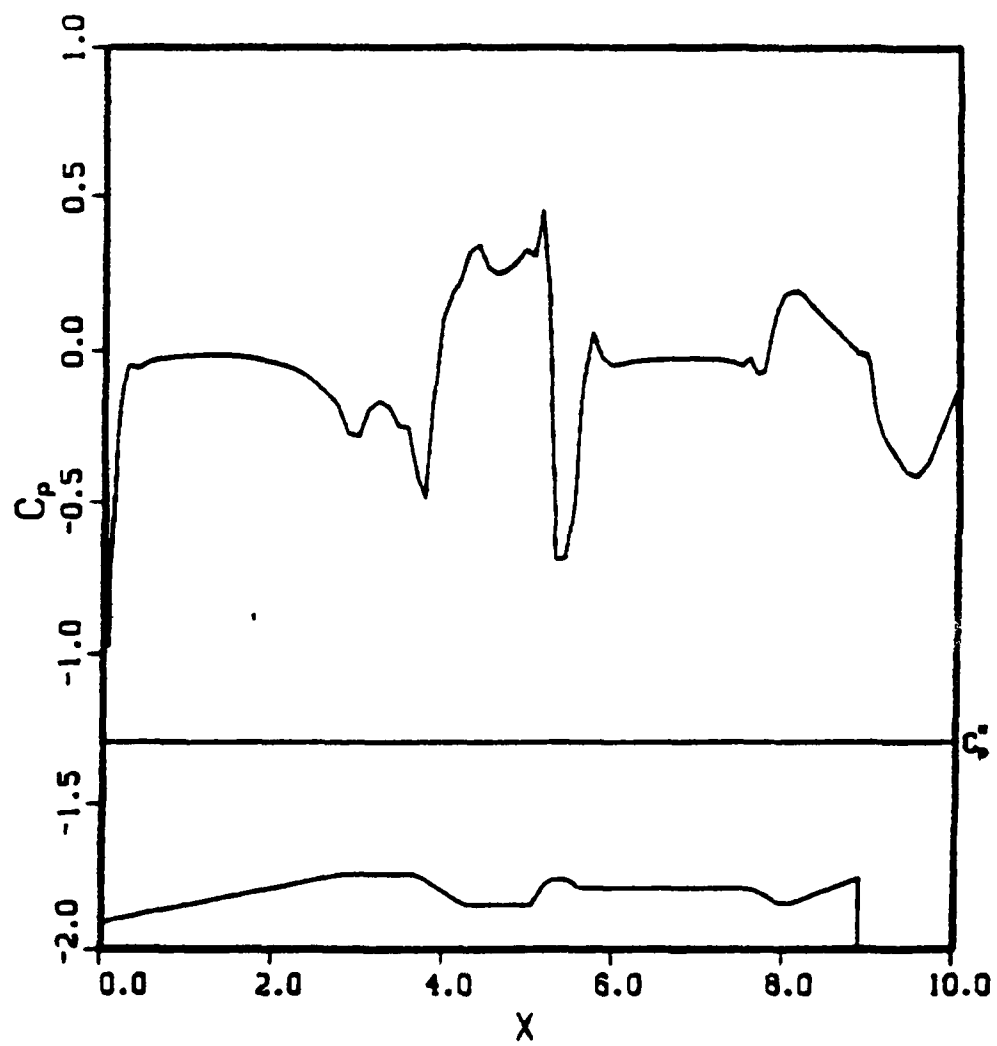


Figure 8. Surface Pressure Distribution,  $M_\infty = 0.5$ ,  $\alpha = 0$ ,  
 $Re = 4.2 \times 10^6/\text{ft}$  (Turbulent)

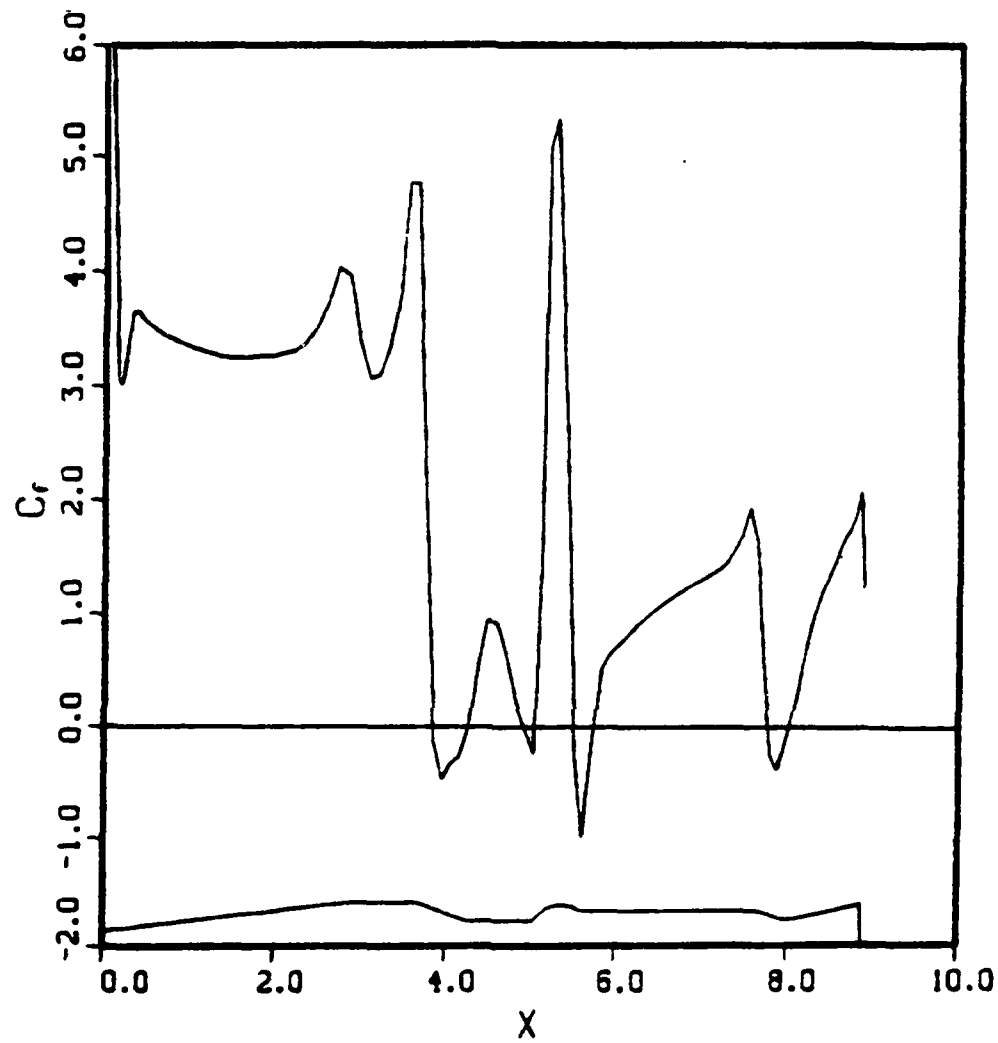


Figure 9. Skin Friction Coefficient Distribution,  $M_\infty = 0.6$ ,  $\alpha = 0$ ,  
 $Re = 4.2 \times 10^6/\text{ft}$  (Turbulent)

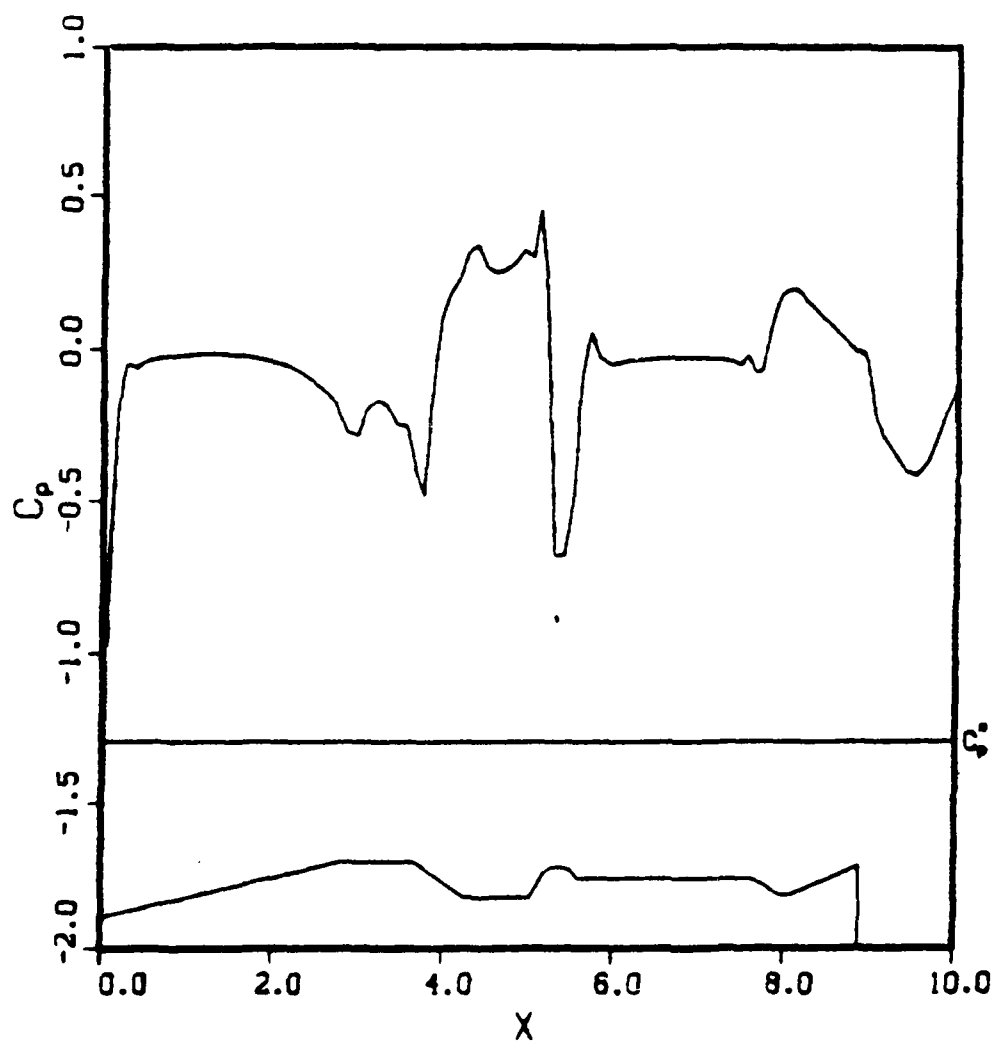


Figure 10. Surface Pressure Distribution,  $M_\infty = 0.6$ ,  $\alpha = 0$ ,  
 $Re = 3.0 \times 10^6/\text{ft}$  (Turbulent)

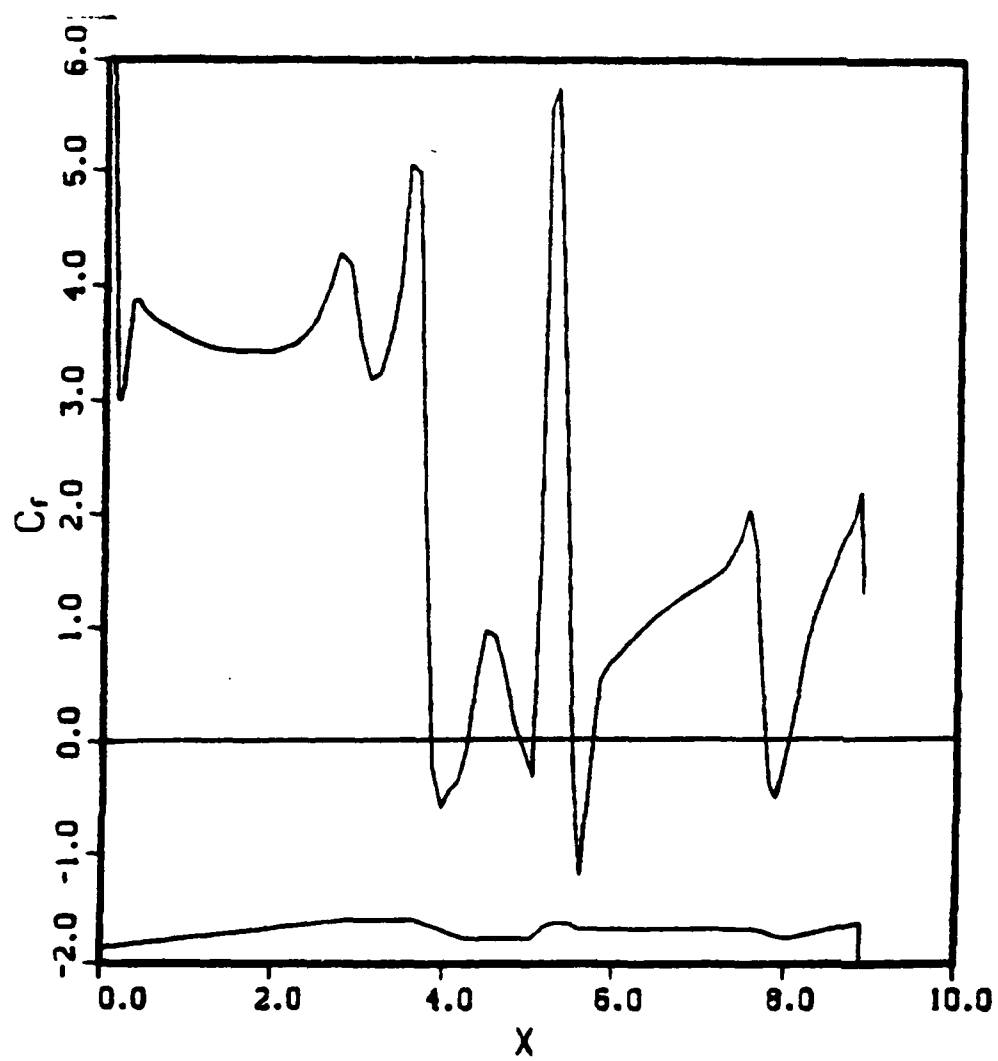


Figure 11. Skin Friction Coefficient Distribution,  $M_\infty = 0.6$ ,  $\alpha = 0$ ,  
 $Re = 3.0 \times 10^6/\text{ft}$  (Turbulent)

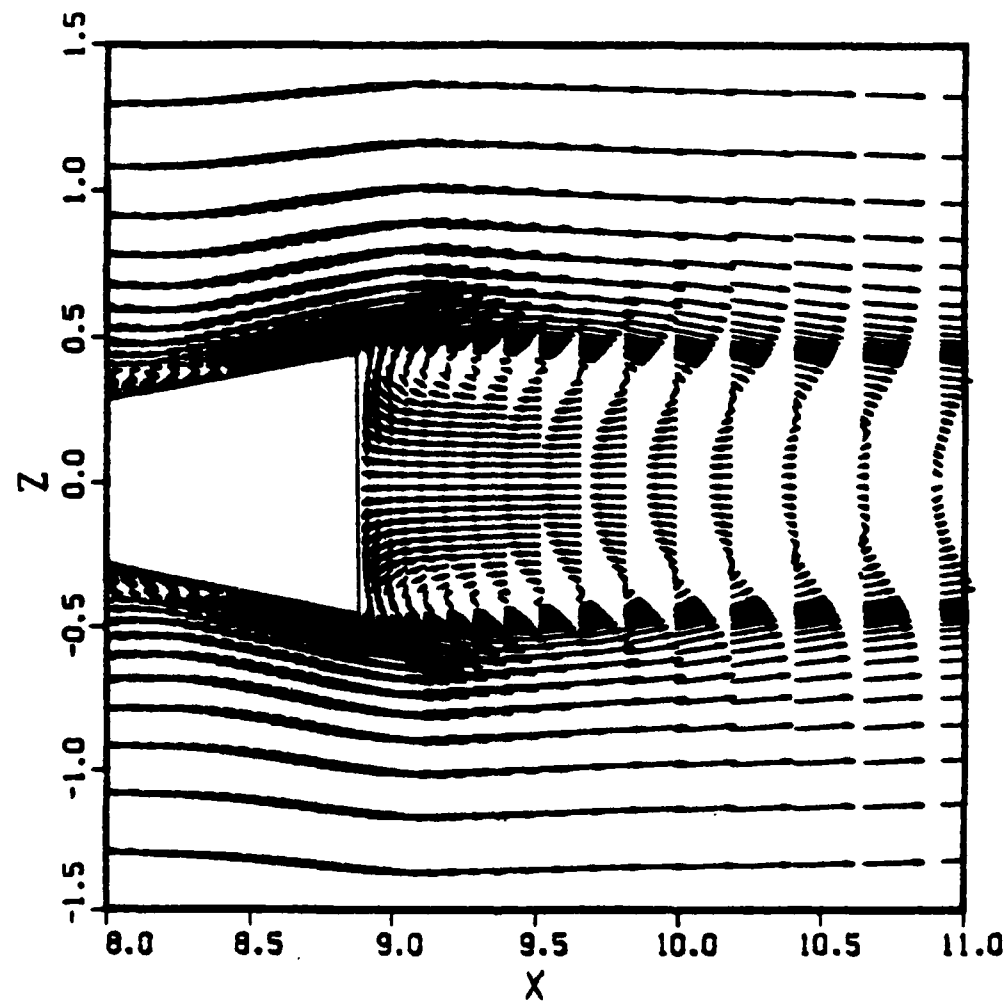


Figure 12. Velocity Vectors in Base Region,  $M_\infty = 0.6$ ,  $\alpha = 0$ ,  
 $Re = 4.2 \times 10^6/\text{ft}$  (Laminar)

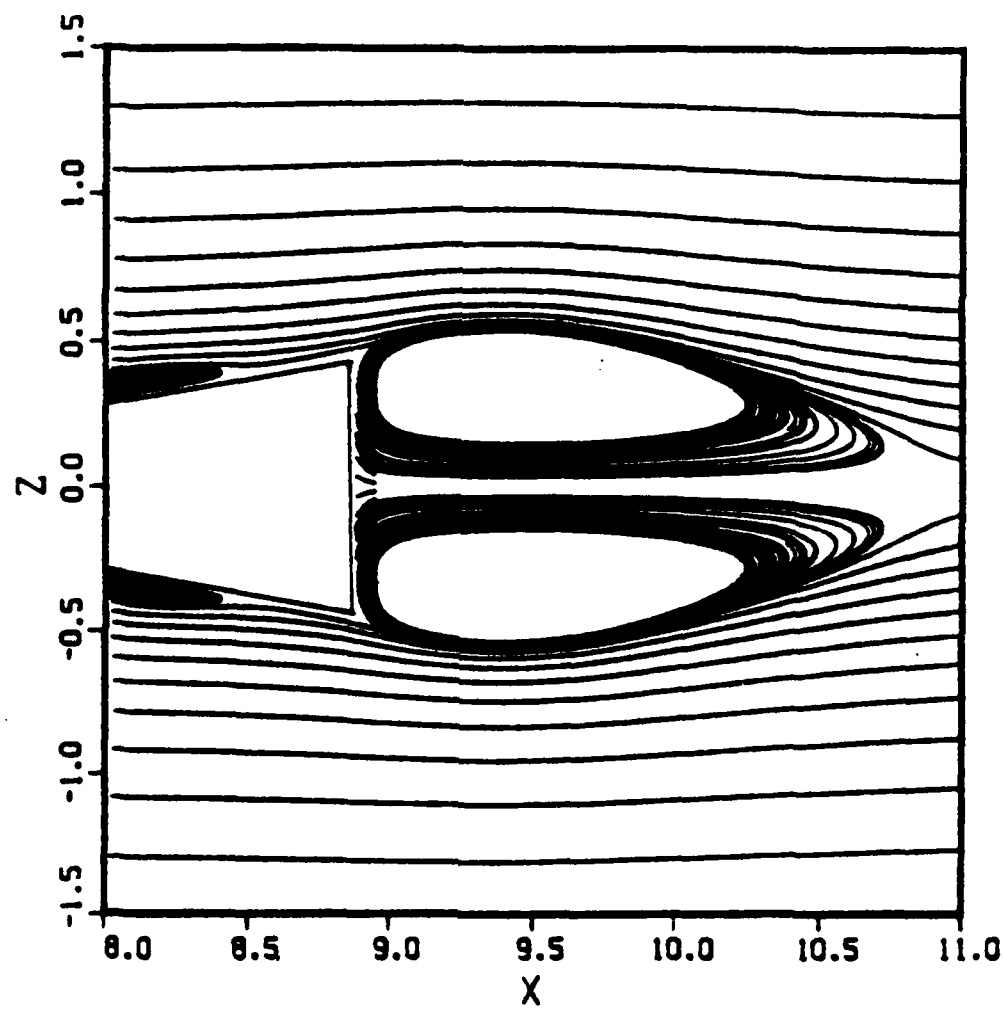


Figure 13. Particle Paths in Base Region,  $M_\infty = 0.6$ ,  $\alpha = 0$ ,  
 $Re = 4.2 \times 10^6/\text{ft}$  (Laminar)

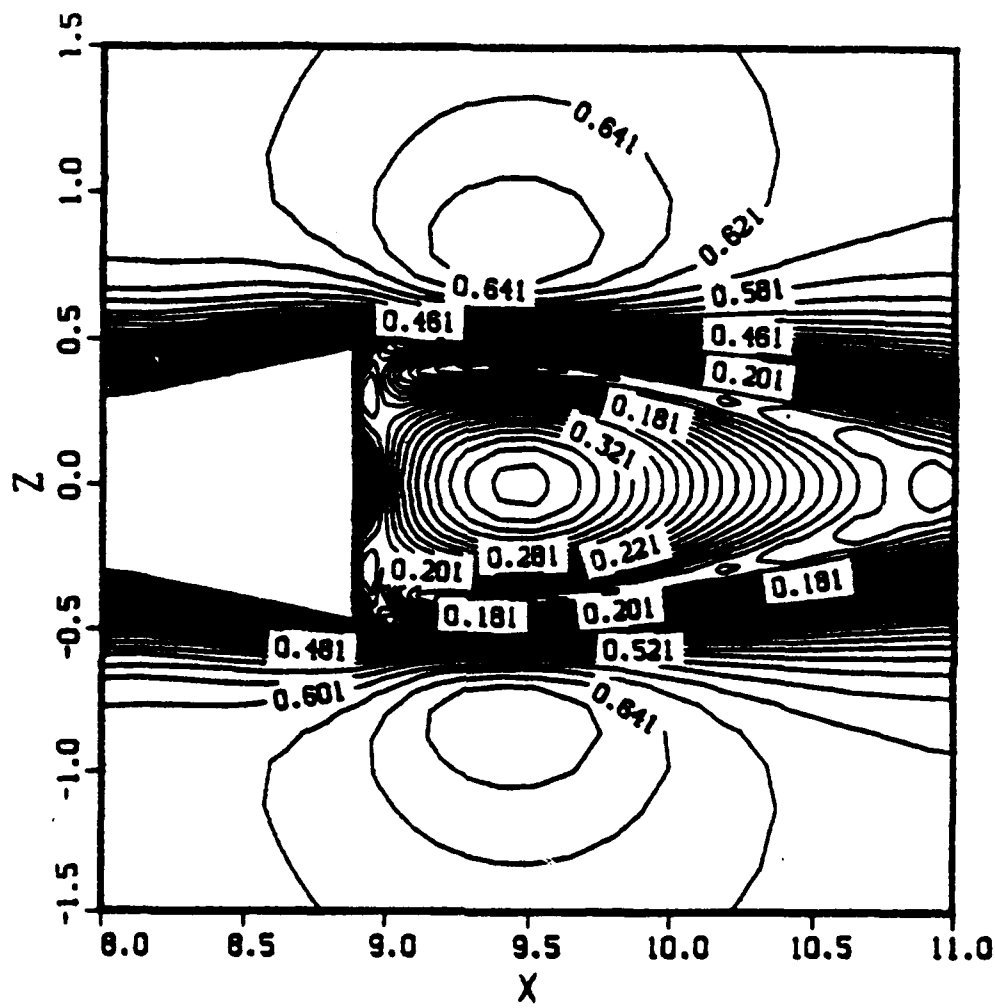


Figure 14. Mach Number Contours in Base Region,  $M_\infty = 0.6$ ,  $\alpha = 0$ ,  
 $Re = 4.2 \times 10^6/\text{ft}$  (Laminar)

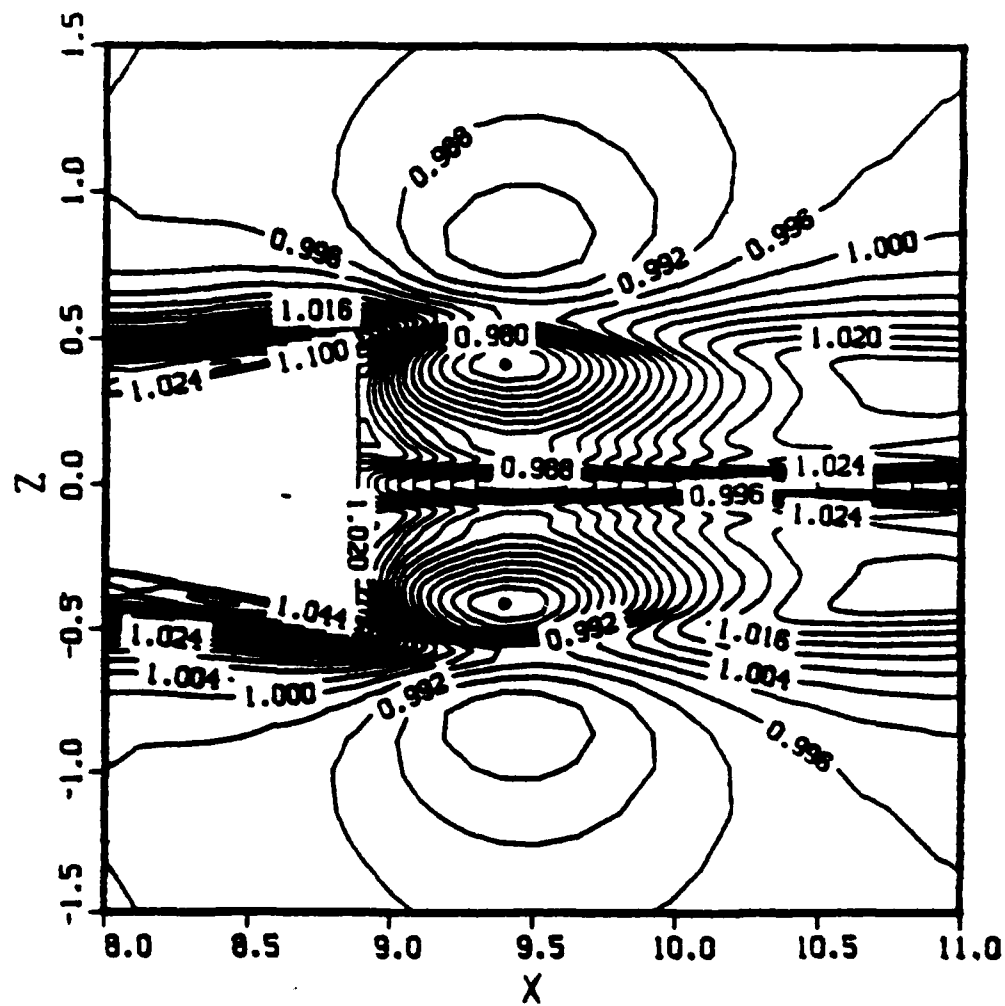


Figure 15. Static Temperature Contours in Base Region,  $M_\infty = 0.6$ ,  $\alpha = 0$ ,  
 $Re = 4.2 \times 10^6/\text{ft}$  (Laminar)

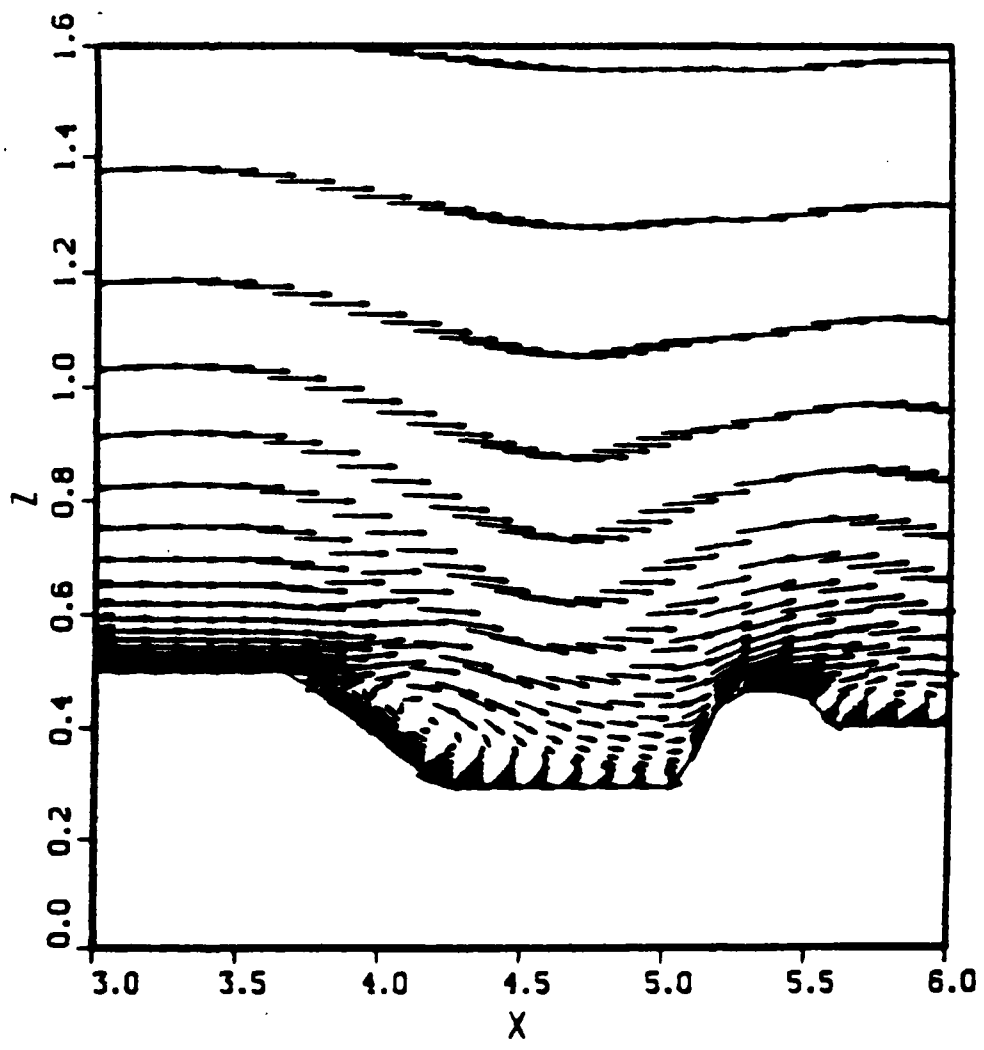


Figure 16. Velocity Vectors,  $M_\infty = 0.6$ ,  $\alpha = 0$ ,  $Re = 4.2 \times 10^6/\text{ft}$  (Laminar)

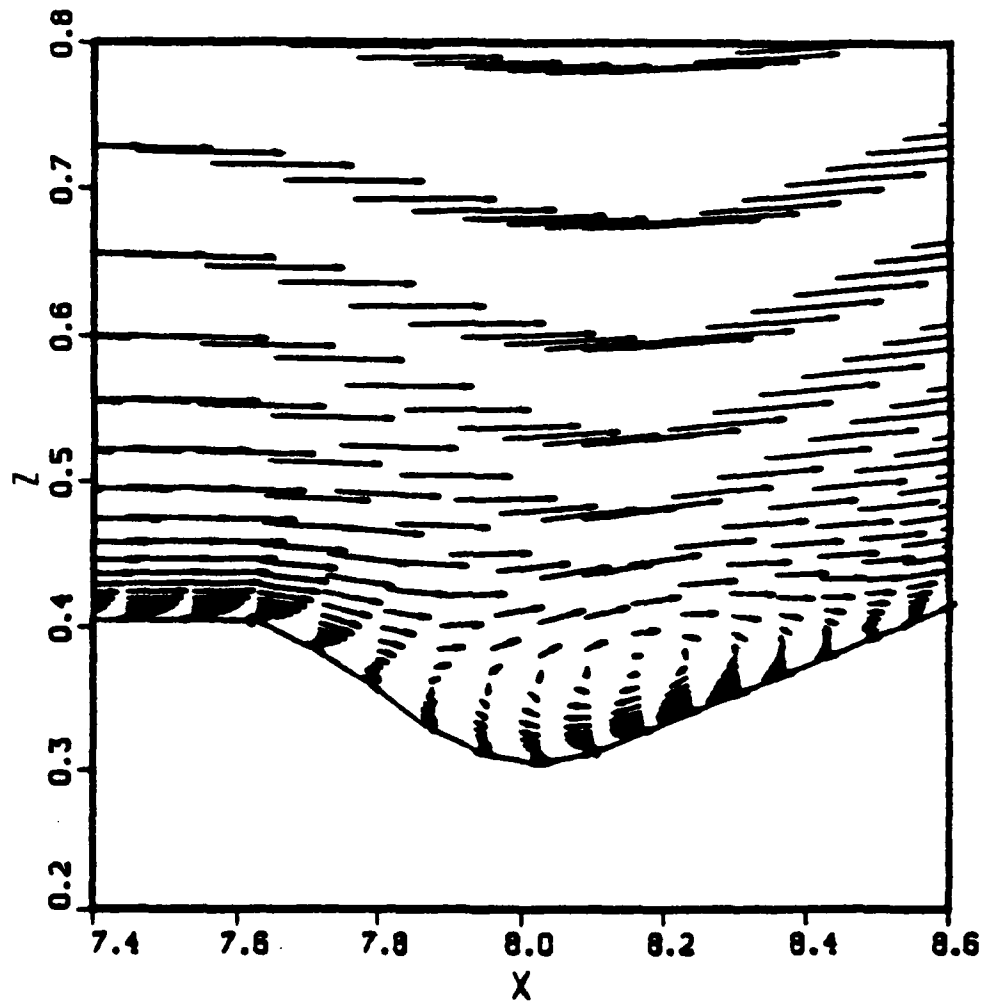


Figure 17. Velocity Vectors,  $M_\infty = 0.6$ ,  $\alpha = 0$ ,  $Re = 4.2 \times 10^6/\text{ft}$  (Laminar)

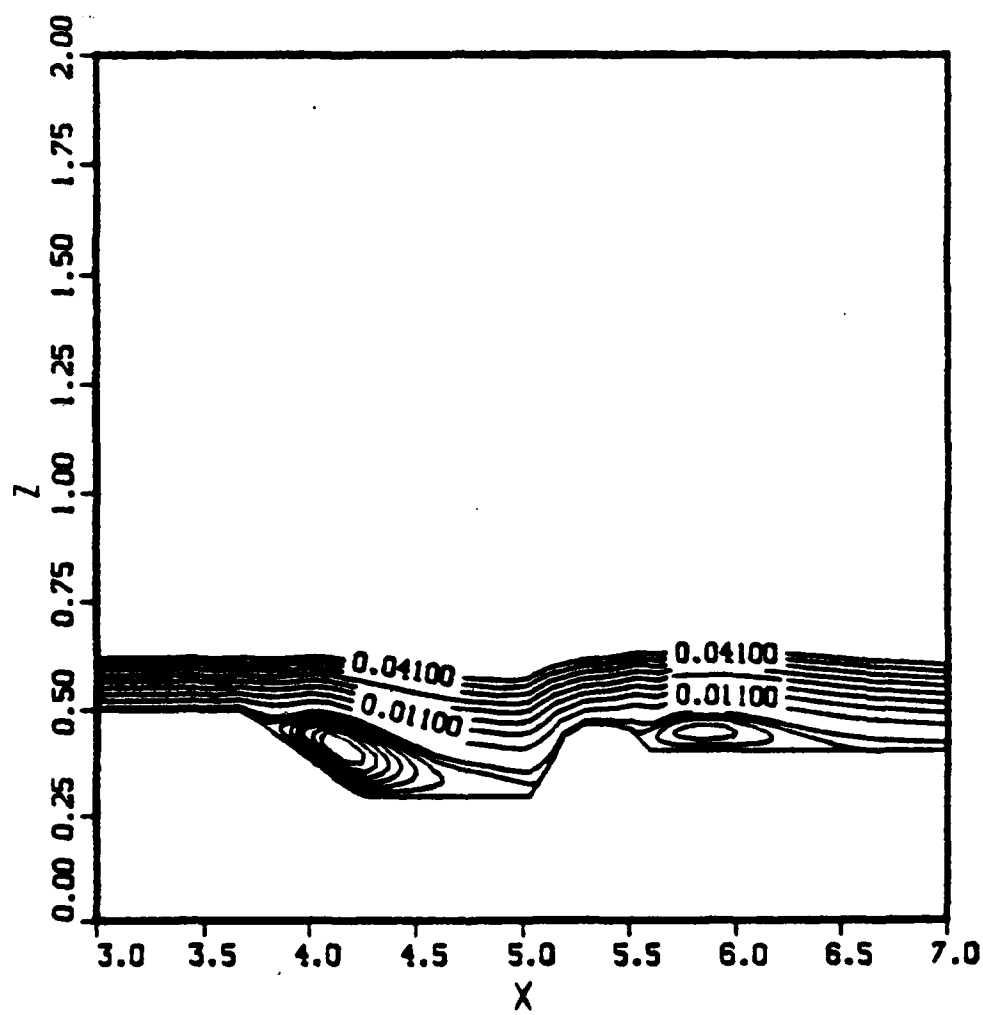


Figure 18. Stream Function Contours,  $M_\infty = 0.6$ ,  $\alpha = 0$ ,  
 $Re = 4.2 \times 10^6/\text{ft}$  (Laminar)

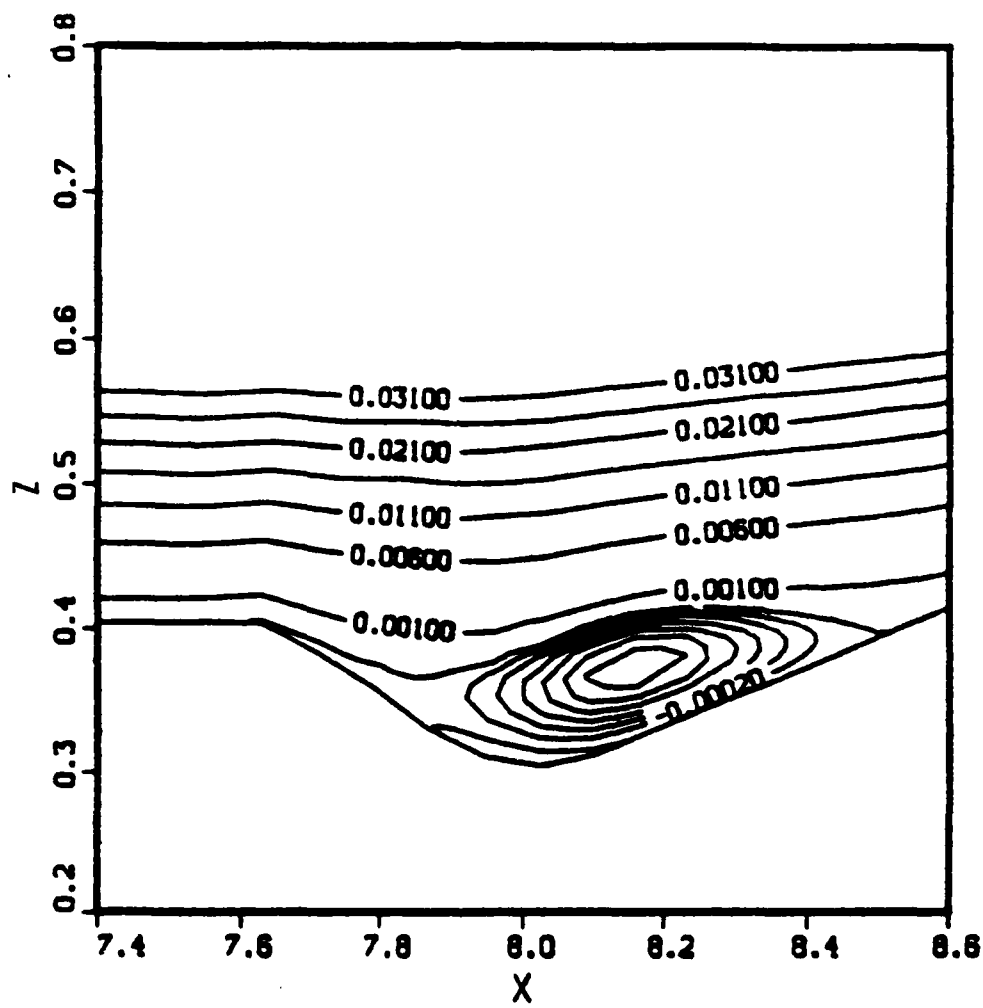


Figure 19. Stream Function Contours,  $M_\infty = 0.6$ ,  $\alpha = 0$ ,  
 $Re = 4.2 \times 10^6/\text{ft}$  (Laminar)

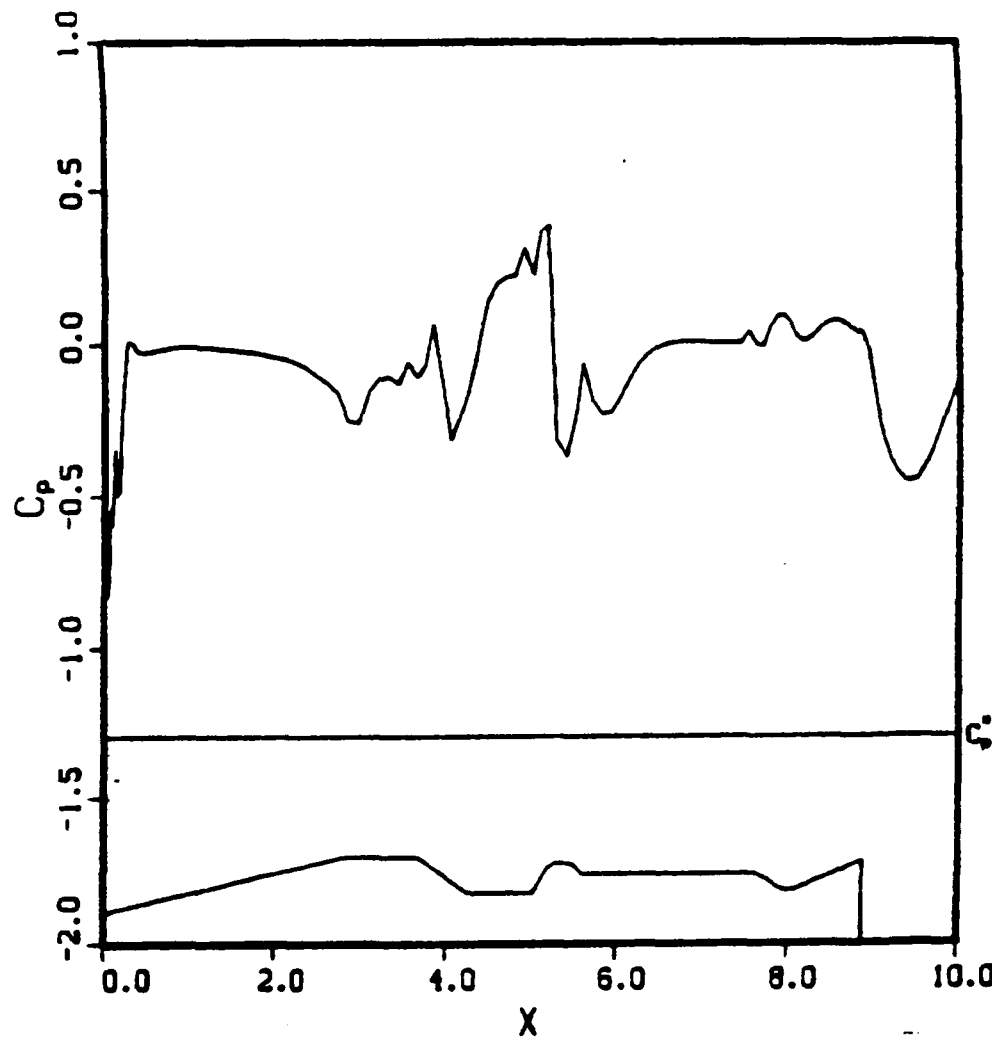


Figure 20. Surface Pressure Distribution,  $M_\infty = 0.6$ ,  $\alpha = 0$ ,  
 $Re = 4.2 \times 10^6/\text{ft}$  (Laminar)

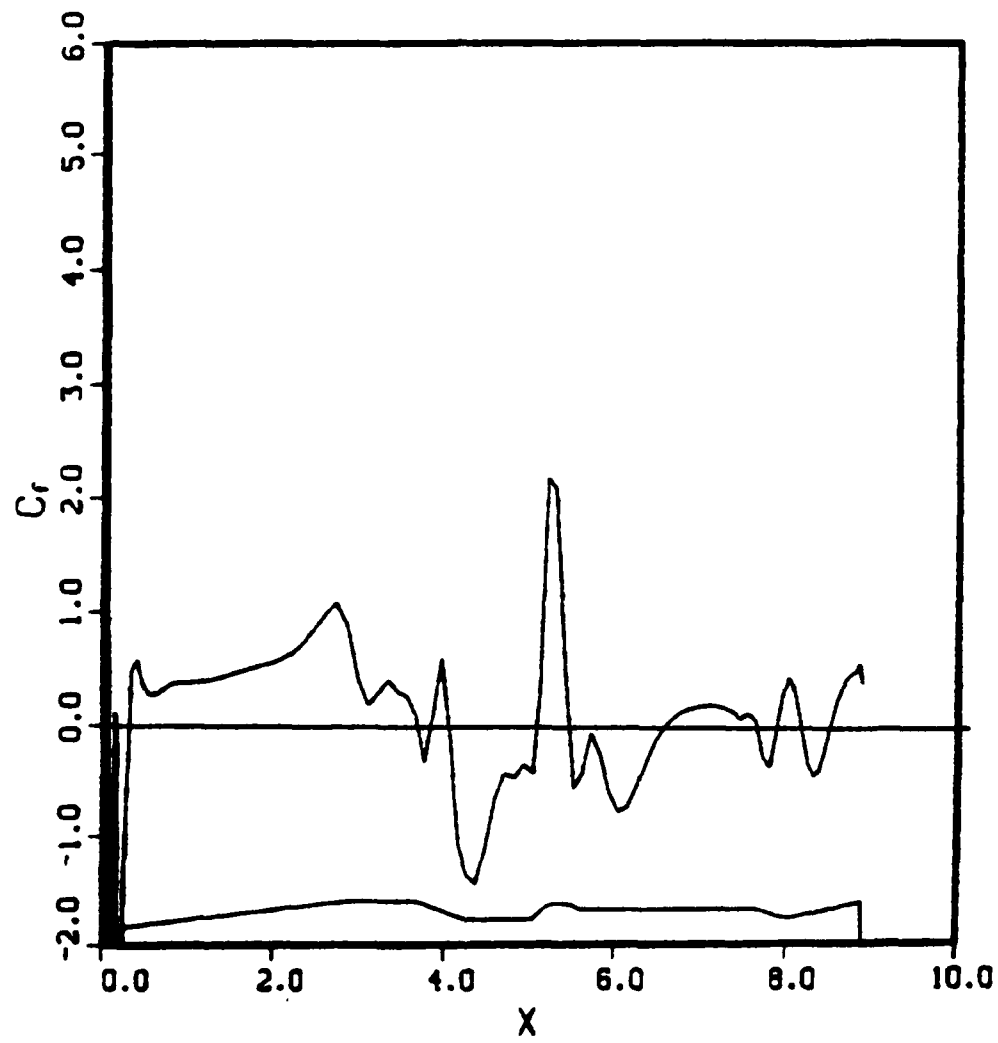


Figure 21. Skin Friction Coefficient Distribution,  $M_\infty = 0.6$ ,  $\alpha = 0$ ,  
 $Re = 4.2 \times 10^6/\text{ft}$  (Laminar)

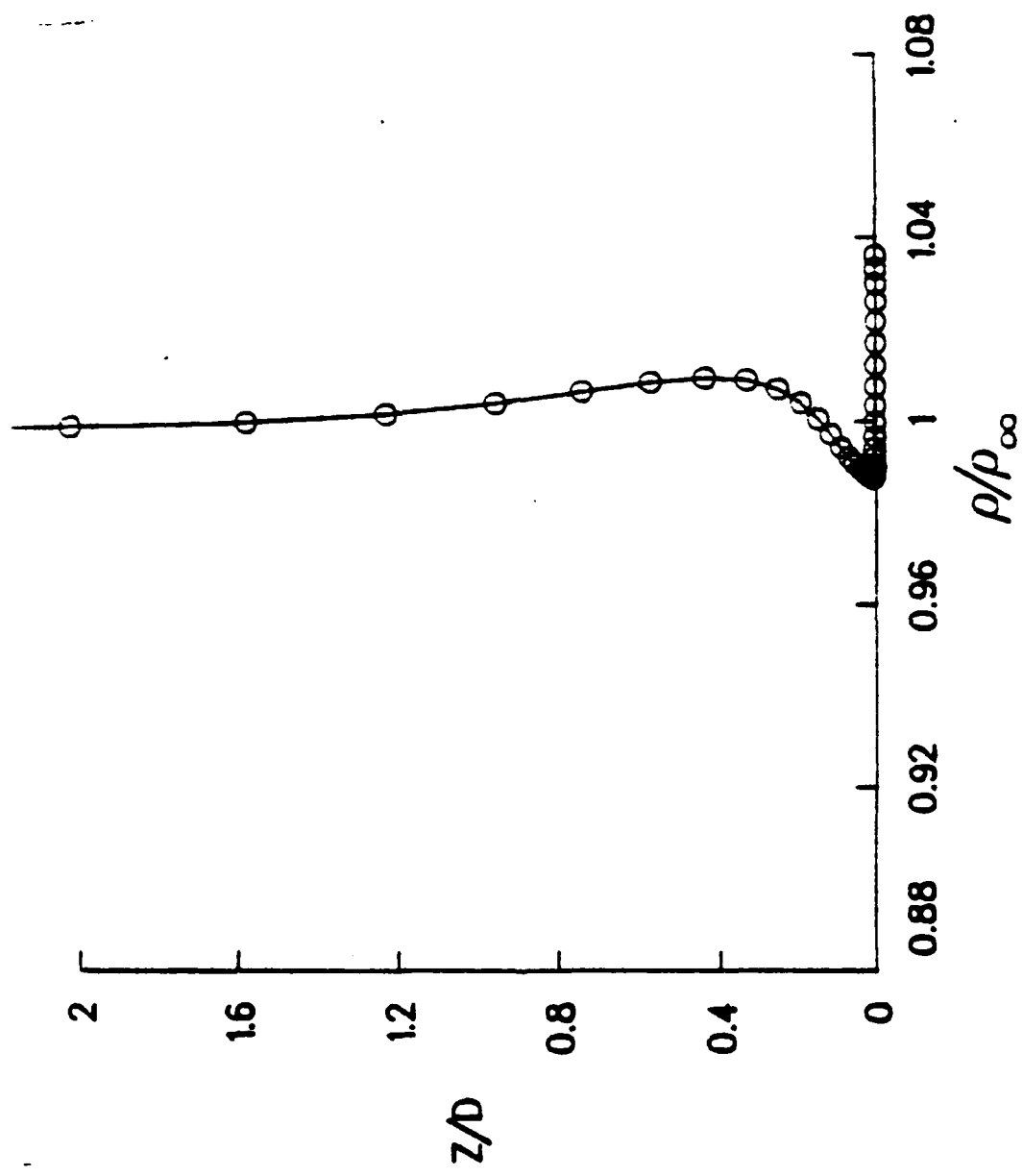


Figure 22. Density Profile,  $M_\infty = .6$ ,  $\alpha = 0$ ,  $x/D = 8.306$

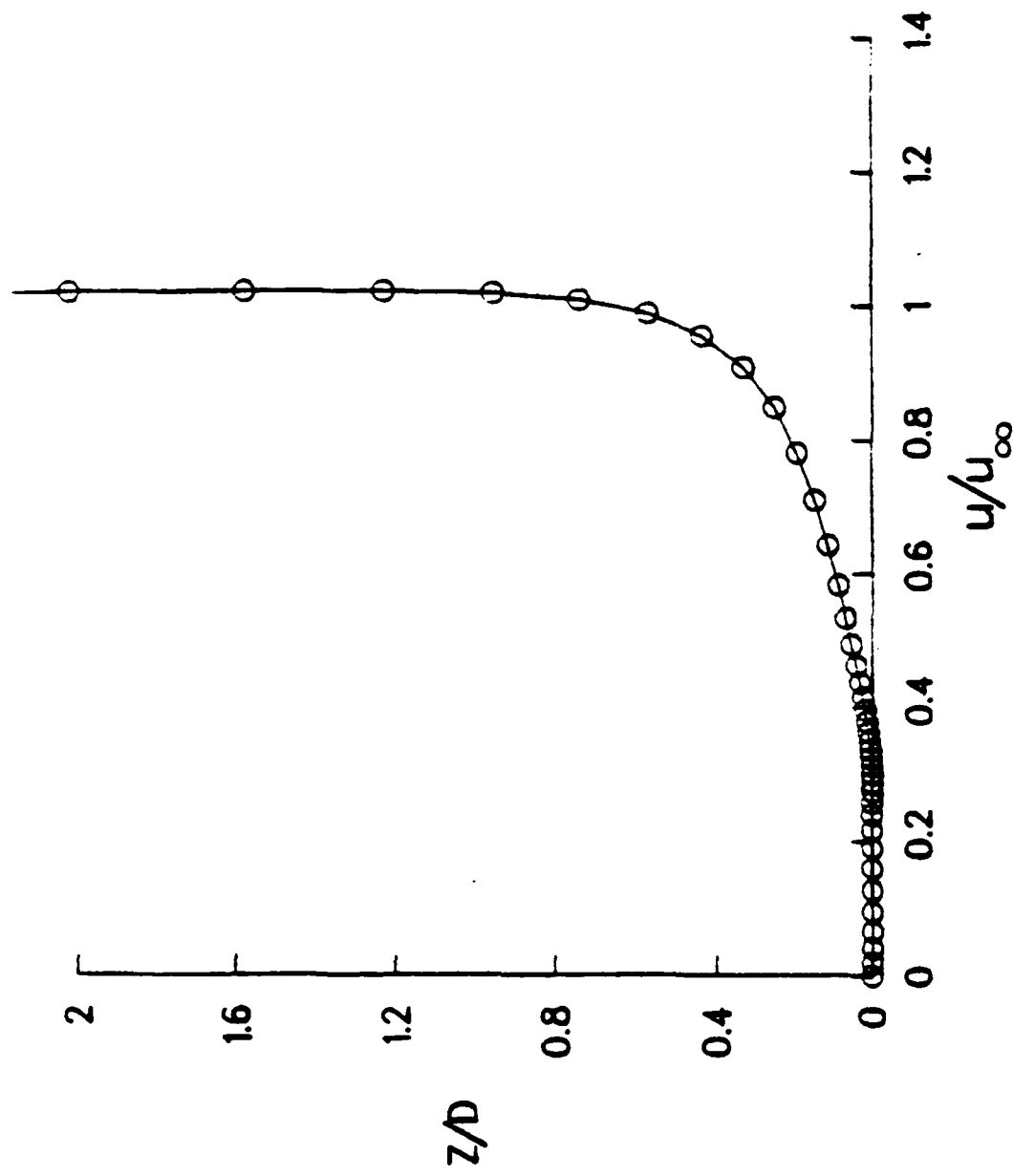


Figure 23.  $x$ -Component of Velocity Profile,  $M_\infty = .6$ ,  $\alpha = 0$ ,  $x/D = 8.306$

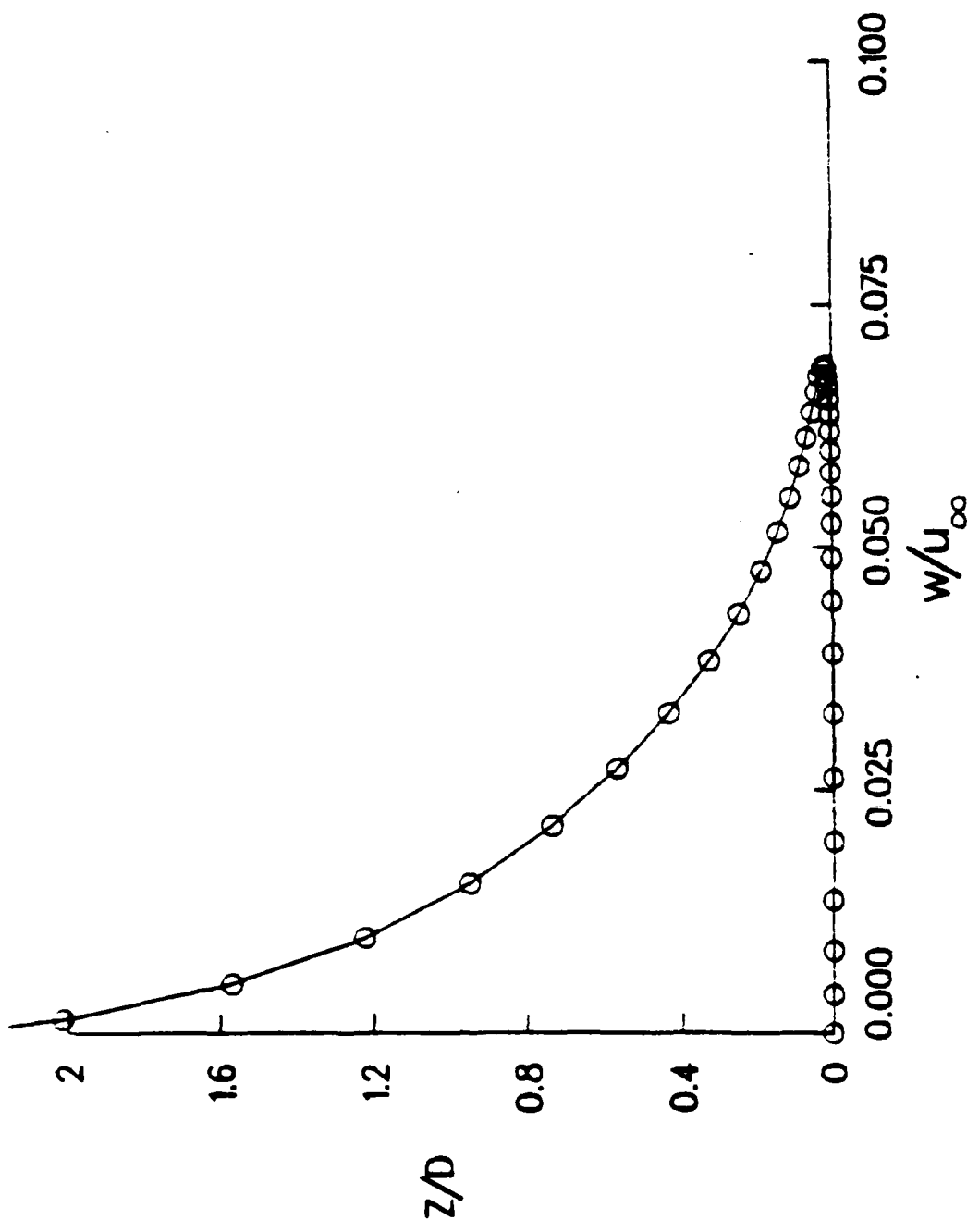


Figure 24. Y-Component of Velocity Profile,  $M_{\infty} = .6$ ,  $\alpha = 0$ ,  $X/D = 8.306$

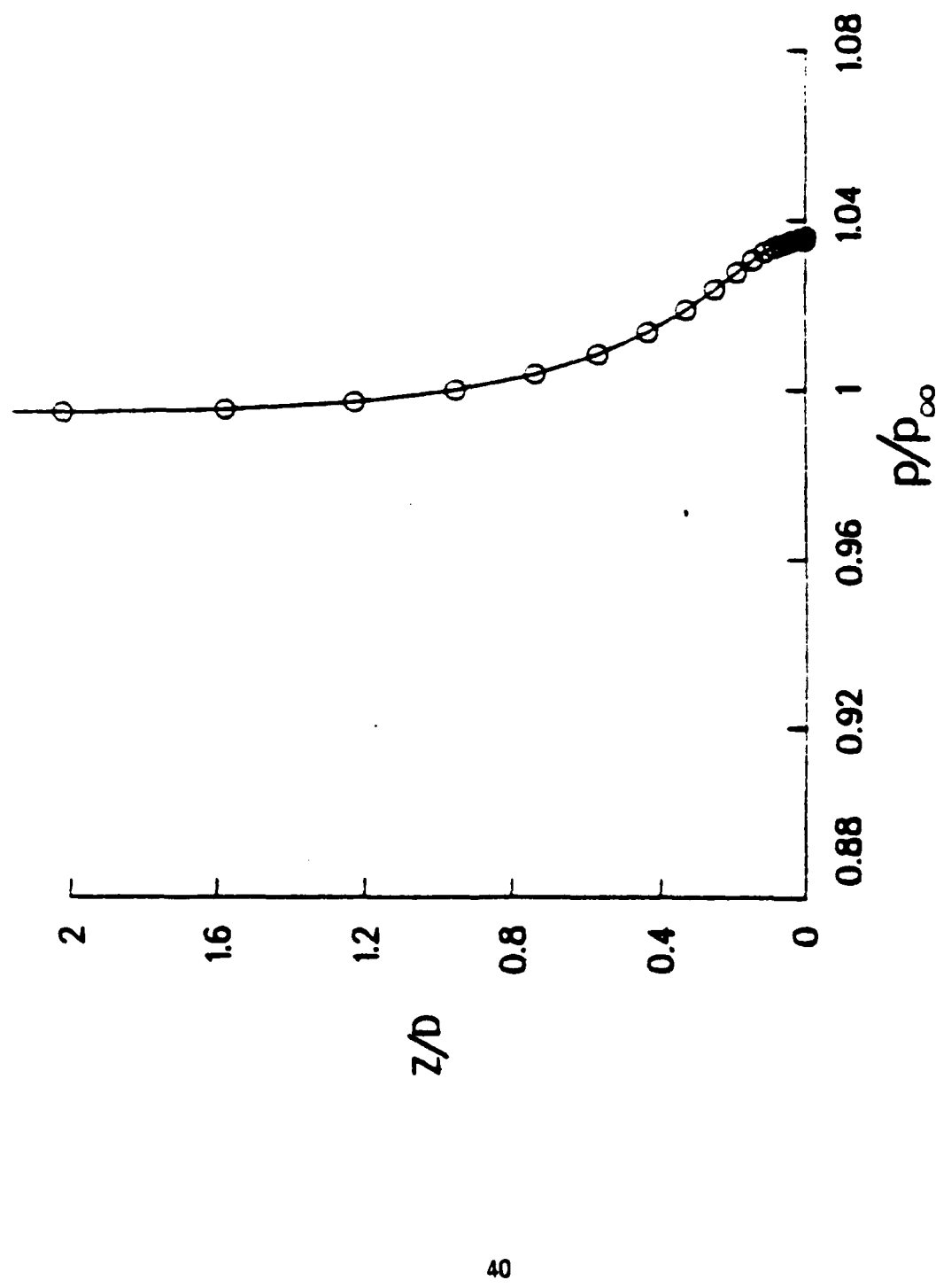


Figure 25. Static Pressure Profile,  $M_a = .6$ ,  $\alpha = 0$ ,  $x/D = 8.306$

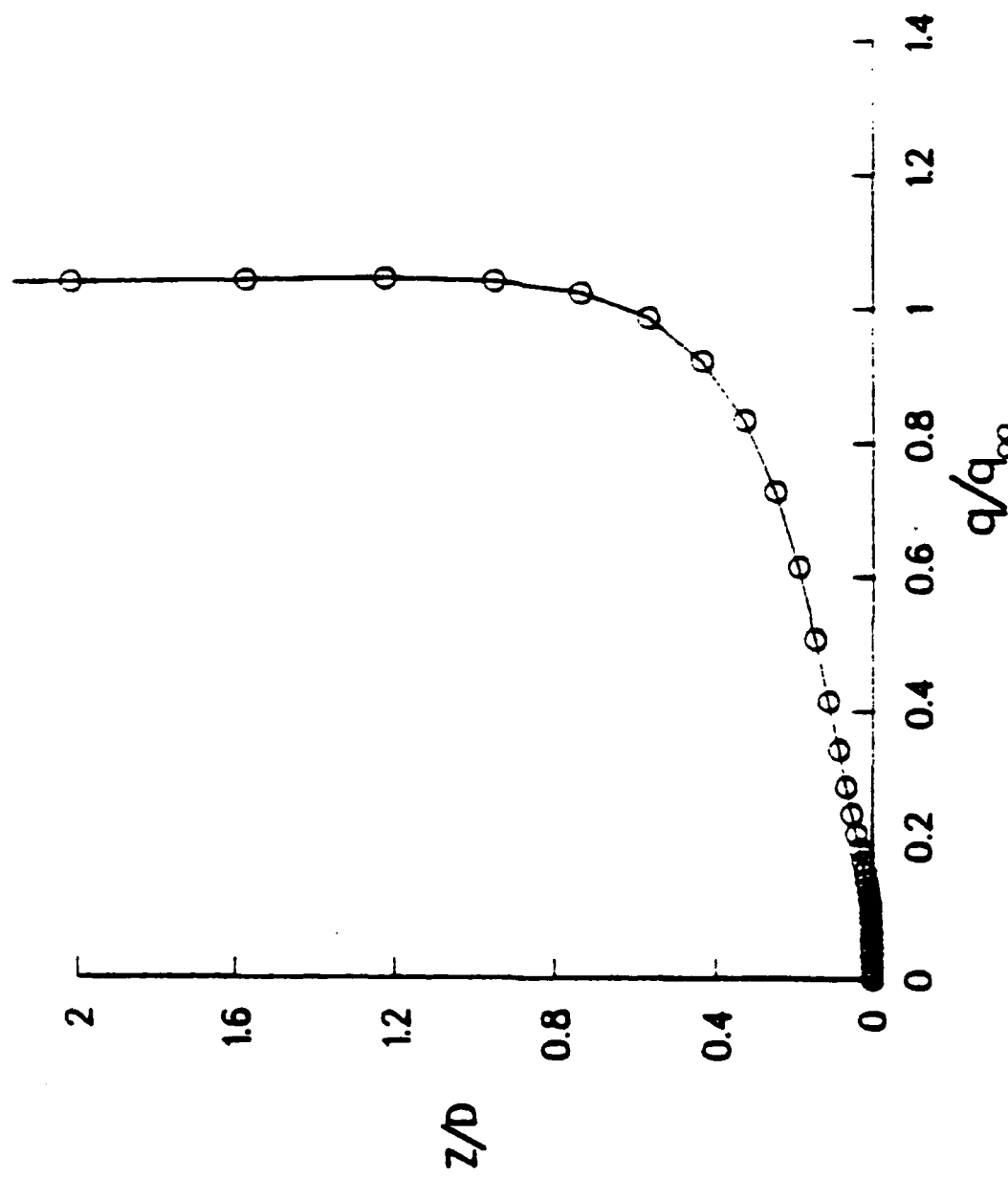


Figure 26. Dynamic Pressure Profile,  $M_{\infty} = .6$ ,  $\alpha = 0$ ,  $x/D = 8.306$

Table 1. Flow Field Data at X/D = 8.306

Z/D	RHO/RINF	U/UINF	W/UINF	P/PINF	Q/QINF
0.00000	1.03619	0.00000	0.00000	1.03619	0.00000
.00004	1.03321	.01940	.00399	1.03619	.00041
.00008	1.02994	.04105	.00845	1.03619	.00181
.00014	1.02614	.06646	.01368	1.03618	.00472
.00022	1.02179	.09581	.01971	1.03617	.00978
.00031	1.01705	.12779	.02628	1.03615	.01731
.00044	1.01223	.16018	.03291	1.03612	.02707
.00060	1.00763	.19064	.03911	1.03605	.03816
.00080	1.00347	.21754	.04450	1.03594	.04948
.00107	.99982	.24027	.04893	1.03577	.06011
.00141	.99671	.25912	.05247	1.03557	.06966
.00186	.99411	.27488	.05533	1.03538	.07816
.00243	.99203	.28850	.05777	1.03528	.08588
.00316	.99043	.30083	.05996	1.03532	.09319
.00412	.98925	.31256	.06196	1.03543	.10045
.00534	.98842	.32427	.06376	1.03556	.10795
.00692	.98787	.33641	.06532	1.03565	.11601
.00896	.98757	.34938	.06663	1.03571	.12493
.01159	.98750	.36353	.06768	1.03573	.13503
.01498	.98763	.37912	.06841	1.03572	.14657
.01935	.98791	.39634	.06872	1.03566	.15986
.02498	.98831	.41548	.06848	1.03553	.17524
.03225	.98883	.43716	.06759	1.03532	.19349
.04160	.98952	.46264	.06604	1.03504	.21611
.05365	.99052	.49394	.06390	1.03469	.24571
.06918	.99203	.53343	.06131	1.03425	.28601
.08919	.99419	.58291	.05838	1.03358	.34120
.11505	.99705	.64250	.05515	1.03246	.41462
.14870	1.00043	.70988	.05158	1.03055	.50681
.19295	1.00391	.78045	.04759	1.02760	.61376
.25183	1.00689	.84828	.04315	1.02356	.72641
.33023	1.00881	.90762	.03826	1.01865	.83251
.43323	1.00928	.95441	.03294	1.01331	.92045
.56605	1.00828	.98713	.02722	1.00806	.98324
.73528	1.00618	1.00682	.02126	1.00334	1.02041
.95004	1.00359	1.01638	.01532	.99948	1.03698
1.22291	1.00118	1.01942	.00978	.99667	1.04054
1.57059	.99939	1.01919	.00504	.99493	1.03813
2.01496	.99842	1.01790	.00139	.99415	1.03449
2.58437	.99817	1.01668	-.00111	.99411	1.03175
3.31445	.99840	1.01579	-.00260	.99452	1.03019
4.24764	.99881	1.01509	-.00336	.99512	1.02918
5.43206	.99917	1.01431	-.00368	.99569	1.02798
6.92126	.99938	1.01325	-.00375	.99615	1.02605
8.77616	.99943	1.01181	-.00366	.99653	1.02319
11.06881	.99939	1.00998	-.00340	.99689	1.01945
13.88611	.99937	1.00778	-.00291	.99738	1.01500
17.33081	.99946	1.00531	-.00214	.99807	1.01011
21.52252	.99968	1.00267	-.00113	.99897	1.00503
26.60690	1.00000	1.00000	0.00000	1.00000	1.00000

## REFERENCES

1. C. J. Nietubicz, T. H. Pulliam, and J. L. Steger, "Numerical Solution of the Azimuthal-Invariant Navier-Stokes Equations," U.S. Army Ballistic Research Laboratory, Aberdeen Proving Ground, Maryland, ARBRL-TR-02227, March 1980. (AD A085716) (Also see AIAA Paper No. 79-0010, January 1979.)
2. J. L. Steger, "Implicit Finite Difference Simulation of Flow about Arbitrary Geometries with Application to Airfoils," AIAA Journal, Vol. 16, No. 7, July 1978, pp. 679-686.
3. T. H. Pulliam and J. L. Steger, "On Implicit Finite-Differences Simulations of Three-Dimensional Flow," AIAA Journal, Vol. 18, No. 2, February 1980, pp. 159-167.
4. R. Beam and R. F. Warming, "An Implicit Factored Scheme for the Compressible Navier-Stokes Equations," AIAA Journal, Vol. 16, No. 4, April 1978, pp. 393-402.
5. B. S. Baldwin and H. Lomax, "Thin-Layer Approximation and Algebraic Model for Separated Turbulent Flows," AIAA Paper No. 78-257, 1978.
6. J. Sahu, C. J. Nietubicz and J. L. Steger, "Numerical Computation of Base Flow for a Projectile at Transonic Speeds," U.S. Army Ballistic Research Laboratory, Aberdeen Proving Ground, Maryland, ARBRL-TR-02495, June 1983. (AD A130293) (Also see AIAA Paper No. 82-1358, August 1982).
7. J. Sahu, C. J. Nietubicz and J. L. Steger, "Navier-Stokes Computations of Projectile Base Flow with and without Base Injection," U.S. Army Ballistic Research Laboratory, Aberdeen Proving Ground, Maryland, ARBRL-TR-02532, November 1983. (AD A135738) (Also see AIAA Paper No. 83-0224, January 1983).

DISTRIBUTION LIST

<u>No. of Copies</u>	<u>Organization</u>	<u>No. of Copies</u>	<u>Organization</u>
12	Administrator Defense Technical Info Center ATTN: DTIC-DDA Cameron Station Alexandria, VA 22304-6145	1	Director US Army Air Mobility Research and Development Command Ames Research Center Moffett Field, CA 94035
1	HQDA DAMA-ART-M Washington, DC 20310	1	Commander US Army Communications - Electronics Command ATTN: AMSEL-ED Fort Monmouth, NJ 07703
1	Commander US Army Materiel Command ATTN: AMCDRA-ST 5001 Eisenhower Avenue Alexandria, VA 22333-0001	1	Commander ERADCOM Technical Library ATTN: DELSD-L (Reports Section) Fort Monmouth, NJ 07703-5301
6	Commander Armament R&D Center US Army AMCCOM ATTN: SMCAR-TDC SMCAR-TSS SMCAR-LCA-F Mr. D. Mertz Mr. A. Loeb Mr. H. Hudgins Mr. E. Friedman Dover, NJ 07801	3	Commander, U.S. Army Missile Command Research, Development & Engineering Ct. ATTN: AMSMI-RD AMSMI-RDK - Dr. B. Walker Mr. R. Deep Redstone Arsenal, AL 35898
1	Commander US Army Armament, Munitions and Chemical Command ATTN: SMCAR-ESP-L Rock Island, IL 61299	1	Director, U.S. Army Missile & Space Intelligence Center ATTN: AIAMS-YDL Redstone Arsenal, AL 35898-5500
1	Director Benet Weapons Laboratory Armament R&D Center US Army AMCCOM ATTN: SMCAR-LCB-TL Watervliet, NY 12189	1	Commander US Army Tank Automotive Command ATTN: AMSTA-TSL Warren, MI 48090
1	Commander US Army Aviation Research and Development Command ATTN: AMSAV-E 4300 Goodfellow Blvd. St. Louis, MO 63120	1	Director US Army TRADOC Systems Analysis Activity ATTN: ATAA-SL White Sands Missile Range, NM 88002
		1	Commander US Army Research Office P. O. Box 12211 Research Triangle Park, NC 27709

DISTRIBUTION LIST

<u>No. of Copies</u>	<u>Organization</u>	<u>No. of Copies</u>	<u>Organization</u>
1	Commander US Naval Air Systems Command ATTN: AIR-604 Washington, D. C. 20360	1	Air Force Armament Laboratory ATTN: AFATL/DLODL Eglin AFB, FL 32542-5000
2	Commander US Naval Surface Weapons Center ATTN: Dr. T. Clare, Code DK20 Dr. F. Moore Dahlgren, VA 22448	2	Director Sandia Laboratories ATTN: Division No. 1331, Mr. H.R. Vaughn Dr. F. Blottner P.O. Box 580 Albuquerque, NM 87184
1	Commander US Naval Surface Weapons Center ATTN: Dr. U. Jettmar Silver Spring, MD 20910	1	AEDC Calspan Field Services ATTN: MS 600 (Dr. John Benek) AAFS, TN 37389
1	Commander US Naval Weapons Center ATTN: Code 3431, Tech Lib China Lake, CA 93555	1	Virginia Polytechnic Institute & State University ATTN: Dr. Clark H. Lewis Department of Aerospace & Ocean Engineering Blacksburg, VA 24061
1	Commander US Army Development and Employment Agency ATTN: MODE-TED-SAB Fort Lewis, WA 98433	1	University of California, Davis Department of Mechanical Engineering ATTN: Prof. H.A. Dwyer Davis, CA 95616
1	Director NASA Langley Research Center ATTN: NS-185, Tech Lib Langley Station Hampton, VA 23365	1	University of Delaware Mechanical and Aerospace Engineering Department ATTN: Dr. J. E. Danberg Newark, DE 19711
4	Director NASA Ames Research Center ATTN: MS-202A-14, Dr. P. Kutler MS-202-1, Dr. T. Pulliam Dr. J. Steger MS-227-8, Dr. L. Schiff Moffett Field, CA 94035	1	University of Florida Dept. of Engineering Sciences College of Engineering ATTN: Prof. C. C. Hsu Gainesville, FL 32611
2	Commandant US Army Infantry School ATTN: ATSH-CD-CSO-OR Fort Benning, GA 31905	1	University of Illinois at Urbana Champaign Department of Mechanical and Industrial Engineering ATTN: Prof. W. L. Chow Urbana, IL 61801
1	AFWL/SUL Kirtland AFB, NM 87117		

DISTRIBUTION LIST

<u>No. of Copies</u>	<u>Organization</u>
1	University of Maryland Department of Aerospace Engr. ATTN: Dr. J. D. Anderson, Jr. College Park, MD 20742
1	University of Notre Dame Department of Aeronautical and Mechanical Engineering ATTN: Prof. T. J. Mueller Notre Dame, IN 46556
1	University of Texas Department of Aerospace Engineering and Engineering Mechanics ATTN: Dr. D. S. Dolling Austin, Texas 78712-1055
<u>Aberdeen Proving Ground</u>	
	Dir, USAMSA ATTN: AMXSY-D AMXSY-MP, H. Cohen
	Cdr, USATECOM ATTN: AMSTE-TO-F
	Cdr, CRDC, AMCCOM ATTN: SMCCR-RSP-A SMCCR-MU SMCCR-SPS-IL
10	Central Intelligence Agency Office of Central Reference Dissemination Branch Room GE-47 HQS Washington, D.C. 20502

### USER EVALUATION SHEET/CHANGE OF ADDRESS

This Laboratory undertakes a continuing effort to improve the quality of the reports it publishes. Your comments/answers to the items/questions below will aid us in our efforts.

1. BRL Report Number \_\_\_\_\_ Date of Report \_\_\_\_\_

2. Date Report Received \_\_\_\_\_

3. Does this report satisfy a need? (Comment on purpose, related project, or other area of interest for which the report will be used.)  
\_\_\_\_\_  
\_\_\_\_\_

4. How specifically, is the report being used? (Information source, design data, procedure, source of ideas, etc.)  
\_\_\_\_\_  
\_\_\_\_\_

5. Has the information in this report led to any quantitative savings as far as man-hours or dollars saved, operating costs avoided or efficiencies achieved, etc? If so, please elaborate.  
\_\_\_\_\_  
\_\_\_\_\_

6. General Comments. What do you think should be changed to improve future reports? (Indicate changes to organization, technical content, format, etc.)  
\_\_\_\_\_  
\_\_\_\_\_

Name \_\_\_\_\_

CURRENT Organization \_\_\_\_\_

ADDRESS Address \_\_\_\_\_

City, State, Zip \_\_\_\_\_

7. If indicating a Change of Address or Address Correction, please provide the New or Correct Address in Block 6 above and the Old or Incorrect address below.

Name \_\_\_\_\_

OLD Organization \_\_\_\_\_

ADDRESS Address \_\_\_\_\_

City, State, Zip \_\_\_\_\_

(Remove this sheet along the perforation, fold as indicated, staple or tape closed, and mail.)

----- FOLD HERE -----

Director  
U.S. Army Ballistic Research Laboratory  
ATTN: SLCBR-DD-T  
Aberdeen Proving Ground, MD 21005-5066

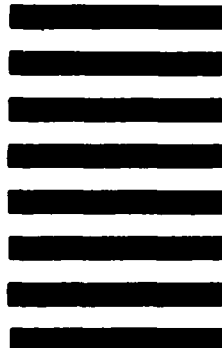


NO POSTAGE  
NECESSARY  
IF MAILED  
IN THE  
UNITED STATES

OFFICIAL BUSINESS  
PENALTY FOR PRIVATE USE, \$300

**BUSINESS REPLY MAIL**  
FIRST CLASS PERMIT NO 12062 WASHINGTON,DC  
POSTAGE WILL BE PAID BY DEPARTMENT OF THE ARMY

Director  
U.S. Army Ballistic Research Laboratory  
ATTN: SLCBR-DD-T  
Aberdeen Proving Ground, MD 21005-9989



----- FOLD HERE -----

FEND

FILMED

3

-86

DTIC